An Eulerian Limited-Area Atmospheric Transport Model

LENNART ROBERTSON AND JOAKIM LANGNER

Swedish Meteorological and Hydrological Institute, Norrkoping, Sweden

MAGNUZ ENGARDT*

Department of Meteorology, Stockholm University, Stockholm, Sweden

(Manuscript received 30 June 1997, in final form 29 January 1998)

ABSTRACT

A limited-area, offline, Eulerian atmospheric transport model has been developed. The model is based on a terrain-following vertical coordinate and a mass-conserving, positive definite advection scheme with small phase and amplitude errors. The objective has been to develop a flexible, all-purpose offline model. The model includes modules for emission input, vertical turbulent diffusion, and deposition processes. The model can handle an arbitrary number of chemical components and provides a framework for inclusion of modules describing physical and chemical transformation processes between different components. Idealized test cases, as well as simulations of the atmospheric distribution of ^{222}Rn, demonstrate the ability of the model to meet the requirements of mass conservation and positiveness and to produce realistic simulations of a simple atmospheric tracer.

1. Introduction

Understanding the distribution and fluxes of various atmospheric trace constituents requires a proper knowledge of atmospheric transport as well as the relevant physical and chemical transformation and deposition processes for the trace species considered. Numerical modeling currently presents a powerful way of analyzing many problems related to atmospheric trace constituents. The increasing power of digital computers as well as a steady improvement in the quality and resolution of meteorological data has led to the development and successful application of three-dimensional atmospheric transport models on a range of scales from local to global. Representative examples of limited-area transport models are, for example, the STEM (Carmichel and Peters 1984), RADM (Chang et al. 1987), and EURAD (Ebel et al. 1991) models. Over the last five years the Swedish Meteorological and Hydrological Institute (SMHI) has developed a limited-area atmospheric transport model called MATCH (Multiple-Scale Atmospheric Transport and Chemistry Modeling System). The work started with the development of a high-resolution (5 km $\times$ 5 km horizontal resolution) model for southern Sweden (Persson et al. 1990). This model was built on a vertical structure with only three model layers: a surface layer with constant thickness, a second layer representing the atmospheric boundary layer, and a third reservoir layer. The height of the interface between layer two and three followed the spatial and temporal variation of the boundary layer height. This three-layer version of MATCH is used in air pollution applications over regions in Sweden up to the size of Sweden. See, for example, Persson et al. (1994), Langner et al. (1995), and Langner et al. (1996).

The need for a model that could be applied over a larger horizontal domain prompted the development of a model with more layers in the vertical. This multilayer version of MATCH has now reached a stage in development when it is used in many different applications inside and outside of SMHI. A proper documentation of the basic transport model is therefore called for. This paper provides a description of the physical concepts on which the MATCH transport model is based and how these are implemented numerically. The results from a number of idealized test cases are presented along with simulations of the radioactive noble gas ^{222}Rn.

The MATCH model is described in section 2 followed by a discussion about balance between atmospheric mass and wind field (section 3). Section 4 presents some tests of the numerical accuracy. The control experiments with ^{222}Rn are described in section 5 and summarized

* Current affiliation: Swedish Meteorological and Hydrological Institute, Norrkoping, Sweden.

Corresponding author address: Dr. Lennart Robertson, Swedish Meteorological and Hydrological Institute, S-601 76 Norrkoping, Sweden.
E-mail: lroberts@smhi.se

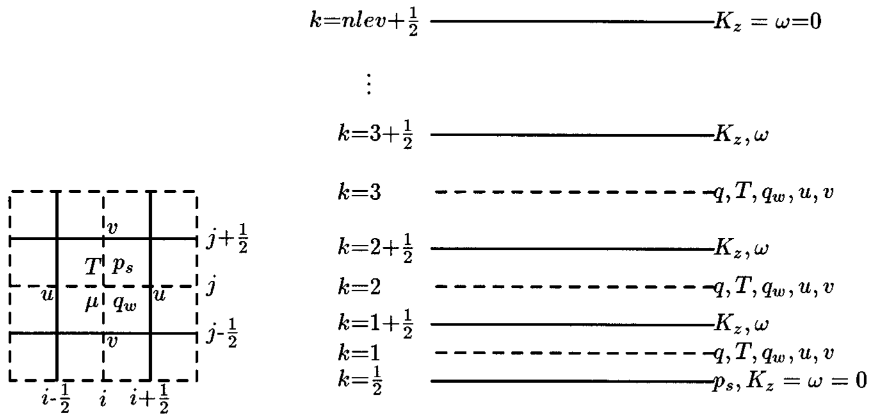

FIG. 1. Staggering of variables in the horizontal (left) and the vertical (right), where u, v, and ω are the wind components; T is the temperature; μ is the mixing ratio of the modeled component; q_w is mixing ratio of water vapor; p_s is the surface pressure; and K_z is the vertical exchange coefficient.

in section 5g. The paper is completed with conclusions in section 6.

2. Model description

a. Model structure

The MATCH transport model is a three-dimensional ''offline'' model, which means that meteorological surface and upper-air data are taken from some external source and fed into the model at regular time intervals, normally every 3 or 6 h. Such data are usually interpolated in time to yield hourly data. Special attention is given to interpolation of the horizontal wind where vector increments are applied (Robertson et al. 1996) The vertical wind is calculated internally to ensure mass consistency of the atmospheric motion (see section 3).

The trace species are represented as mass mixing ratios and prescribed boundary mixing ratios are treated in the same fashion as meteorological data, that is, read at regular time intervals and interpolated in time (see section 2g).

The model design is flexible with regard to the horizontal and vertical resolution, principally defined by the input weather data, and allows for an arbitrary number of chemical compounds. The model is written in η (or hybrid) vertical coordinates that is a linear combination of pressure p and σ vertical coordinates, where the pressure at any level is defined as

$$p_k = a_k + b_k p_s, \tag{1}$$

where p_s is the surface pressure. The coefficients a_k and b_k are expected to be given by the input meteorological data and defined in a way that constant pressure levels appear at the top of the model and sigma levels at the bottom. The horizontal wind components are staggered on an Arakawa C grid, and the vertical wind and exchange coefficients are staggered in the vertical; see Fig. 1.

b. Time splitting

The physical processes that have to be considered for the fate of a trace species in the atmosphere are the injection pathways of anthropogenic and/or natural emissions into the atmosphere (A_Q), transport by the mean fluid motion ($A_u + A_v + A_\omega$) and turbulent eddies (A_T), transformation by chemical reactions (A_{CH}), and depletion by gravitational settling and by wet and dry deposition processes (A_D). The trace species are considered nonbuoyant (except during the very initial phase of release when buoyancy may be accounted for), and the input weather data are assumed to represent some timescale longer than the lifetime of turbulent eddies, which then have to be treated in a parametric way. The time-split procedure outlined in Eqs. (2a) and (2b) is applied, where the mixing ratios, μ, are updated for each process sequentially:

$$\mu^* = \mu^t + A_Q \tag{2a}$$

and

$$\mu^{t+\Delta t} = A_{CH}(A_u + A_v + A_\omega)A_D A_T \mu^*. \tag{2b}$$

Here, μ^* is the mixing ratio with the emission increment for the time step added, and A_T, A_D, etc. are the linear operators of the above-mentioned processes. For nonlinear chemistry Eq. (2b) is split into one linear and one nonlinear part, but the general time-split principle is the same. The advection is split into one-dimensional advection processes for each direction. Note that the advective step is operating on the same mixing ratio field in all directions. This procedure is chosen to minimize numerical errors for smoothly varying long-lived tracers such as CO_2. The approach will conserve a uniform tracer distribution as demonstrated in section 4a. We have not yet implemented alternating of the various operators, that is, reversing the order every even time step, which may improve the accuracy.

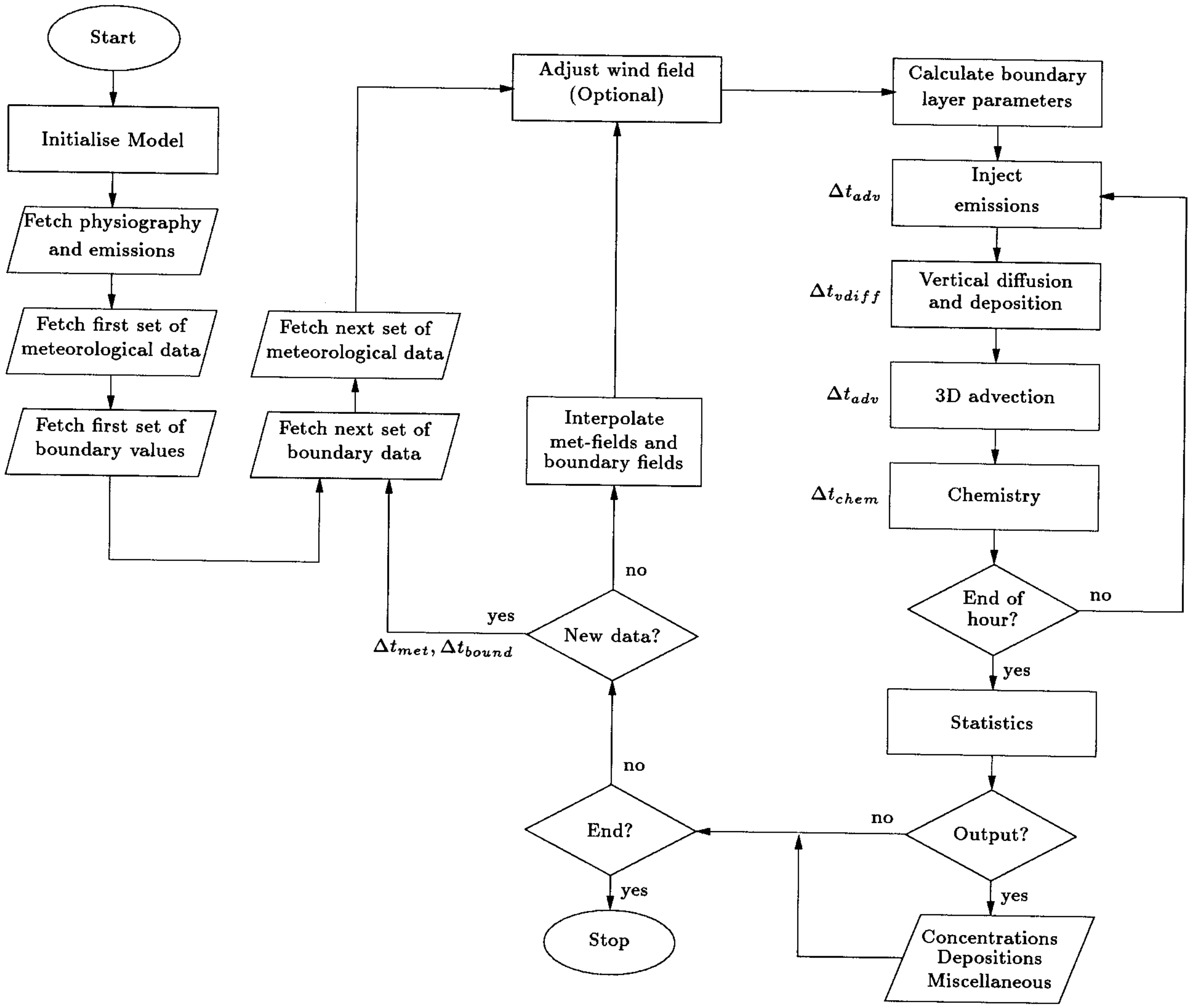

FIG. 2. Data flow and time stepping in the MATCH model. Substepping may take place for vertical diffusion (and deposition) and in the chemistry module with time steps Δt_{vdiff} and Δt_{chem}, respectively. Fetching new meteorology and boundary values may occur at different time intervals (Δt_{met} and Δt_{bound}, respectively).

There are several time steps involved in the data flow through the model. First, there is the large time step over which new weather data (Δt_{met}) and boundary mixing ratios (Δt_{bound}) are read. The second step is the "interpolated" period (usually 1 h); the third, is the advective time step (Δt_{adv}), substepping over vertical diffusion (Δt_{vdiff}), and the chemical reaction scheme (Δt_{chem}). Figure 2 shows the various time stepping as implemented in MATCH.

c. Basic equations

In a Eulerian framework the mass conservation for a given volume is determined by the integrated exchange with the surroundings across the volume boundary and the integrated contribution from the internal stationary sources and sinks. With pressure vertical coordinates, under the hydrostatic assumption, this continuity equation is given by,

$$\frac{\partial}{\partial t}\int_{\Omega} \mu \, d\Omega = \oint_{A} (-\mathbf{v}_n \cdot \mu)\, dA + \int_{\Omega} s \, d\Omega, \quad (3)$$

where Ω is the volume of the grid cell, $d\Omega$ is $dx\,dy\,dp$, A is the area of the grid-cell boundary, μ is the instantaneous mixing ratio of the compound, $\mathbf{v}_n = (u_n, v_n, \omega_n)$ is the instantaneous fluid velocity that is normal to the grid-cell boundary (defined positive when directed outward from the cell), and s is the sum of the instantaneous internal sources and sinks. Splitting the variables into mean and turbulent parts, $\mu = \overline{\mu} + \mu'$, $\mathbf{v}_n = \overline{\mathbf{v}}_n + \mathbf{v}'_n$, and $s = \overline{s} + s'$, respectively, and applying Reynolds averaging procedure yields

$$\frac{\partial}{\partial t}\int_{\Omega}\overline{\mu}\,d\Omega = \oint_A (-\overline{\mathbf{v}}_n\cdot\overline{\mu} - \overline{\mathbf{v}'_n\cdot\mu'})\,dA + \int_{\Omega}\overline{s}\,d\Omega, \tag{4}$$

where $\overline{\mathbf{v}'_n\cdot\mu'}$ is the three-dimensional turbulent flux intensity across the grid-cell boundary. For a discrete grid cell volume, $\Delta x\Delta y\Delta p$, the continuity equation reads

$$\frac{\partial}{\partial t}\tilde{\mu}\Delta x\Delta y\Delta p = \oint_A (-\overline{\mathbf{v}}_n\cdot\overline{\mu} - \overline{\mathbf{v}'_n\cdot\mu'})\,dA + \tilde{s}\Delta x\Delta y\Delta p \tag{5}$$

or if $\partial\Delta x\Delta y\Delta p/\partial t = 0$,

$$(\tilde{\mu}^{t+\Delta t} - \tilde{\mu}^t)\Delta x\Delta y\Delta p = \int_t^{t+\Delta t}\left[\oint_A\left(-\overline{\mathbf{v}}_n(\tau)\cdot\overline{\mu}(\tau) - \overline{\mathbf{v}'_n(\tau)\cdot\mu'(\tau)}\right)dA + \tilde{s}(\tau)\Delta x\Delta y\Delta p\right]d\tau, \tag{6}$$

where $\tilde{\mu}$ and $\tilde{s}$ represent the discrete grid-cell average of mixing ratio, and sources and sinks, respectively. The notation of mean and discrete values will be omitted hereafter. The conversion to η coordinates is straightforward by the substitution $\Delta p = \partial p/\partial\eta\Delta\eta$, and for the vertical velocity $\omega = \dot{p} = \dot{\eta}\partial p/\partial\eta$.

d. Advection

A numerical transport scheme should satisfy several desired properties, such as being conservative, transportive, local, and computationally efficient (Williamson 1991; Rasch and Williamson 1990). The transport scheme in MATCH is based on the Bott scheme (Bott 1989a,b), which fulfills most of these properties. Bott further developed a family of one-dimensional positive definite and mass conservative Eulerian advection schemes suggested by Crowley (1968) and Tremback et al. (1987). Those schemes have been expanded fully into two dimensions by Rasch (1994) and Hólm (1995). The scheme implemented in MATCH is a generalization of the class of mass conservative schemes suggested by Bott (1989a,b) to arbitrary grid selections by means of primitive functions described in the appendix.

We apply the concept of operator splitting into one-dimensional transport problems. For brevity only transport in one selected direction, the x direction, is described hereafter. Following the notations by Bott (1989a) the discretized continuity equation regarding advection in one-dimension is given by

$$\mu_t^{t+\Delta t}\Delta x_i\Delta y_i\Delta p_i = \mu_t^t\Delta x_i\Delta y_i\Delta p_i - (F_{i+1/2} - F_{i-1/2}), \tag{7}$$

where μ_i is the discrete grid-cell average mixing ratio for the volume $\Delta x_i\Delta y_i\Delta p_i$, and $F_{i\pm1/2}$ is the integrated advective flux across the cell interfaces at $x_{i\pm1/2}$. From Eq. (6) the advective flux at $x_{i+1/2}$ could be described by

$$F_{i+1/2} = \int_t^{t+\Delta t}\Delta y_{i+1/2}\Delta p_{i+1/2}u_{i+1/2}(\tau)\mu_{i+1/2}(\tau)\,d\tau. \tag{8}$$

Here $u_{i+1/2}$ and $\mu_{i+1/2}$ are mean values over the cell interface $\Delta y_{i+1/2}\Delta p_{i+1/2}$. A similar expression holds for the cell interface flux $F_{i-1/2}$. For a constant wind field the transport is equivalent to a rigid body motion, and the flux across the cell wall equals the integrated mass along the upstream distance $\delta x = u\Delta t/\Delta x$ (Crowley 1968). In a context of nondimensional coordinates and splitting the flux in two parts, outflow from and inflow to the grid cell across the interface yields

$$F_{i+1/2} = \Delta y_{i+1/2}\Delta p_{i+1/2}\left[\Delta x_i\int_{\zeta(x_{i+1/2})-c^+}^{\zeta(x_{i+1/2})}\mu(\zeta)\,d\zeta - \Delta x_{i+1}\int_{\xi(x_{i+1/2})}^{\xi(x_{i+1/2})+c^-}\mu(\xi)\,d\xi\right], \tag{9}$$

where the first term on the right-hand side is the outflow from the grid cell and the second term is the inflow, $\zeta(x) = x/\Delta x_i$ and $\xi(x) = x/\Delta x_{i+1}$ are nondimensional coordinates, and c is the Courant number where $c^+ = 0.5(|u_{i+1/2}| + u_{i+1/2})\Delta t/\Delta x_i$ and $c^- = 0.5(|u_{i+1/2}| - u_{i+1/2})\Delta t/\Delta x_{i+1}$, respectively, positive or zero dependent on flow direction. Each of the integrals in Eq. (9) can be split in two parts as, for example,

$$\int_{\zeta(x_{i+1/2})-c^+}^{\zeta(x_{i+1/2})}\mu(\zeta)\,d\zeta = \int_0^{\zeta(x_{i+1/2})}\mu(\zeta)\,d\zeta - \int_0^{\zeta(x_{i+1/2})-c^+}\mu(\zeta)\,d\zeta, \tag{10}$$

thus, the difference between two instances of the primitive function of μ that are solved by a Lagrangian polynomial approximation from discrete integral values, described in the appendix. For constant grid spacing the above approach coincides with the area-preserving scheme (Bott 1989b). The advantages of the proposed algorithm are threefold. First, the implementation of this algorithm is trivial; second, the algorithm is inherently applicable to nonuniform gridspacing. Third, the algorithm proves to be computationally more efficient (~10% less floating-point operations when comparing fifth-order polynomial schemes). Other aspects as monotonicity and nonoscillatory, as addressed by, for example, Bott (1992), are not implemented so far.

This approach is applied in the horizontal with a fifth-order polynomial scheme. In the vertical a first or zero-order (upstream) scheme is applied. Flux limitation, as proposed by Bott (1989a), is applied regarding all the fluxes in three dimensions.

Flow-dependent boundary conditions are applied. On the outflow boundary the gradient is prescribed (von Neumann condition) with an assumed zero gradient in the mixing ratio distribution over the boundary. On inflow a Dirichlet condition is applied with the prescribed boundary values assumed to be an infinite reservoir outside the domain.

e. Boundary layer parameterizations

Boundary layer processes, such as dry deposition fluxes and turbulent vertical mixing in the boundary layer, are parameterized by means of the three primary parameters, surface friction velocity (u_*), surface sensible heat flux (H_0), and the boundary layer height (z_{PBL}), from which some secondary parameters are derived such as the convective velocity scale (w_*) and the Monin–Obukhov length (L). The sensible heat flux is given by the surface energy balance equation utilizing formulations suggested by van Ulden and Holtslag (1985) for land areas and ice-covered sea, and Burridge and Gadd (1977) for open sea areas.

The boundary layer height is based on a bulk Richardson number approach (Holtslag et al. 1995) for unstable conditions, $H_0 > 0$, where the boundary layer height is defined at the height where the bulk Richardson number, Ri, reaches a critical value, $\mathrm{Ri}_{\mathrm{cr}} = 0.25$. The bulk Richardson number at height z is defined as

$$\mathrm{Ri}(z) = \left(\frac{gz}{\theta_1}\right)\left(\frac{\theta_z - \theta_0}{|\mathbf{v}_H|_z^2}\right), \tag{11}$$

where

$$\theta_0 = \theta_1 + 8.5\frac{H_0}{\rho_1 c_{\mathrm{pd}} w_m}, \tag{12a}$$

and

$$w_m = (u_*^3 + 0.6 w_*^3)^{1/3}, \tag{12b}$$

where g is the acceleration of gravity, $\theta_{1,z,0}$ are the potential temperature at the first model level, at height z, and at the surface, respectively. Here, $\mathbf{v}_H$ is the horizontal wind vector, ρ_1 is the density of air at the first model level, c_{pd} is the specific heat of dry air, and w_* is the convective velocity scale. For neutral and stable conditions, $H_0 \le 0$, a formulation proposed by Zilitinkevich and Mironov (1996) is used:

$$(a_1 z_{\mathrm{PBL}})^2 + a_2 z_{\mathrm{PBL}} = 1 \tag{13a}$$

or

$$z_{\mathrm{PBL}} = \frac{2}{(a_2^2 + 4a_1^2)^{1/2} + a_2}, \tag{13b}$$

where

$$a_1 = \frac{f}{C_n u_*} \tag{14a}$$

and

$$a_2 = \frac{1}{C_s L} + \frac{N}{C_i u_*} + \frac{|f|^{1/2}}{C_{sr}(u_* L)^{1/2}} + \frac{|Nf|^{1/2}}{C_{ir} u_*}. \tag{14b}$$

Here N is the Brunt–Väisälä frequency, f is the Coriolis parameter, and the coefficients $C_n = 0.5$, $C_s = 10$, $C_i = 20$, $C_{sr} = 1.0$, and $C_{ir} = 1.7$ (see Zilitinkevich and Mironov 1996 for more details).

f. Vertical diffusion and deposition processes

The horizontal diffusive fluxes are assumed to be small and neglected in the current setup. Only the vertical turbulent mixing is accounted for. Transport by deep convection is not considered so far. A first-order approximation of the turbulent flux intensity from mixing length theory is utilized,

$$\overline{\omega'\mu'} = g\rho K_z \frac{\partial\mu}{\partial z} = -(g\rho)^2 K_z \frac{\partial\mu}{\partial p}, \tag{15}$$

where K_z is the turbulent exchange coefficient yet to be determined. Mass conservation with regard to vertical turbulent mixing [cf. Eq. (6)] then reads,

$$\mu_k^{t+\Delta t}\Delta x\Delta y\Delta p = \mu_k^t \Delta x\Delta y\Delta p + \Delta x\Delta y \int_t^{t+\Delta t} \left\{\left[(g\rho)^2 K_z \frac{\partial\mu(\tau)}{\partial p}\right]_{k+1/2} - \left[(g\rho)^2 K_z \frac{\partial\mu(\tau)}{\partial p}\right]_{k-1/2}\right\} d\tau, \tag{16}$$

with the lower boundary condition ($k = 1$),

$$\left[(g\rho)^2 K_z \frac{\partial\mu(\tau)}{\partial p}\right]_{1/2} = g\rho v_d \mu(\tau), \tag{17}$$

where k is the vertical index of the grid cell, and the indices $k + ½$ and $k - ½$ refer to the upper and lower grid-cell boundaries in the vertical, respectively, and v_d is the dry deposition velocity representative for the lowest model layer. The latter is derived from 1-m dry deposition velocities commonly found in the literature transformed to represent the lowest model layer following standard procedures, see, for example, Langner and Rodhe (1991). In the present implementation, the lower boundary condition (17) is calculated explicitly before the vertical diffusion. Equation (16) is reformulated by introducing a turbulent Courant number,

$$\mathcal{K} = \frac{(g\rho)^2 K_z \Delta t}{(\Delta p)^2}, \tag{18}$$

and solved in a semi-implicit fashion (see Robertson et al. 1996 for more details).

Three different formulations of the exchange coefficient, K_z, are applied. The exchange coefficient within the boundary layer follows from suggestions by Holtslag et al. (1995) for neutral and stable conditions,

$$K_z(z) = \frac{ku_* z}{\phi_H(z, z_0, L)}(1 - z/z_{\rm PBL})^2, \qquad (19)$$

where $\phi_H(\ )$ is the similarity profile proposed by Businger et al. (1971). In the convective case, limited by $-z_{\rm PBL}/L \geq 4$ or $u_*/u_* \leq 2.3$ (Holtslag et al. 1995), the turnover time $z_{\rm PBL}/w_*$ is utilized to determine the turbulent Courant number,

$$\mathcal{K} = 1 - \left[\exp\left(\frac{-w_*\Delta t}{z_{\rm PBL}}\right)\right], \qquad (20)$$

which asymptotically approaches the case of rapid vertical mixing ($\mathcal{K} = 1$). Above the boundary layer, K_z is defined explicitly from mixing length theory as

$$K_z = l^2\frac{\partial|\mathbf{v}_H|}{\partial z}, \qquad (21)$$

where the mixing length l is kept constant. In the standard set up of MATCH, l is set to zero.

Wet deposition is described as a linear dependency of the precipitation rate and treated implicitly:

$$\mu^{t+\Delta t} = \mu^t - \Lambda P^t(\alpha\mu^{t+\Delta t} + \beta\mu^t)\Delta t, \qquad (22)$$

where Λ is the scavenging coefficient (s^{-1} h mm^{-1}), P^t is the precipitation rate (mm h^{-1}), $\alpha = 0.692$, and $\beta = 0.308$ (Robertson et al. 1996). Vertical transport by gravitational settling is treated by an upstream scheme with compound dependent sedimentation velocities.

g. Emission and boundary conditions

The basic version of the MATCH transport model includes modules for inclusion of area emissions of the simulated species. Emissions can be introduced at any vertical height in the model and at different heights simultaneously.

Emissions are initially distributed in the vertical based on a Gaussian plume formulation (Berkowicz et al. 1986) evaluated at a downwind distance of $s = u_h\Delta t$, where u_h is the wind speed at the effective plume height. If desired, standard plume-rise calculations (Berkowicz et al. 1986) can be performed based on stack parameters (stack diameter, effluent temperature, and volume flux) that are given as input to the model. It is also possible to specify diurnal variation in the emissions as well as variations between weekdays. The emissions that enter the model calculations are updated every hour to account for temporal variations and the influence of stability on the plume-rise and initial spread calculations.

In some applications the capability to specify mixing ratios on the boundaries of the model domain is required. Boundary conditions can be specified either as a constant value for each boundary (the four sides and the top of the model domain) or can be read from external files. In the case of using external files it is possible to update the boundary mixing ratios at any regular time interval, which then are linearly interpolated in time. This possibility is useful when performing one-way nesting between a large-scale, for example, global model, and a high-resolution MATCH model on a limited area.

3. Adjustment of unbalanced wind fields

Depending on the source of meteorological data, the three-dimensional wind field may not be in exact balance with the mass field, that is, the continuity equation for air may not be exactly fulfilled. This can cause large errors in the calculated vertical wind field and thus in the distribution of the tracer. There are several possible sources for such errors. In particular we note the following:

- low accuracy of the stored meteorological data,
- spatial interpolation errors, and
- time interpolation errors.

Spatial interpolation errors arise when the data are transformed from one spatial representation to another before use. For example, this is the case when using data from global spectral models, such as the European Centre for Medium-Range Forecasts (ECMWF) model. Time interpolation errors are introduced when the meteorological data are interpolated in time from, for example, 6 to 1 h in the offline model. Depending on the particular application, these errors may or may not be of significance. In applications for trace species with short residence times, typically days to weeks, direct output from numerical weather prediction (NWP) models is usually balanced enough to be used directly without modification in an offline model. For tracers with longer residence times the relative importance of errors in the wind field increases, and an adjustment procedure is called for. To maintain a flexible model, an optional adjustment module, based on the method proposed by Heimann and Keeling (1989), has been built into the MATCH transport model (see Fig. 2). The method adjusts the horizontal wind field so that the vertically integrated airmass divergence matches the surface pressure tendency. The vertical wind field is also calculated in this process. See Robertson et al. (1996) for further details.

4. Simple test cases

The numerical properties of the transport model outlined in the preceding sections can be illustrated with a few simple test simulations. The following three types of tests will be discussed:

- transport of a passive tracer with constant initial distribution and constant boundary values,
- transport of a passive tracer with zero initial distribution and constant upper boundary, and
- transport of a passive tracer from a point source.

a. Constant initial distribution and constant boundaries

Figure 3 shows the result from a 48-h simulation of a passive tracer over the period 1200 UTC 23 October 1994 to 1200 UTC 25 October 1994. The model was initialized with a constant mixing ratio of 1000 ppt(m) with the same value specified on all the model boundaries throughout the simulation. The meteorological data were taken from the operational HIRLAM 2.5 model at SMHI (Källén 1996). The horizontal resolution is about 55 km with 16 levels in the vertical. Meteorological data were read every 6 h and were interpolated to 1-h time resolution within MATCH, using the adjustment procedure referred to in section 3. The time step was 300 s for advection and vertical diffusion. Since there are no sources or sinks, the mixing ratio should stay constant in this case. The model is able to keep the mixing ratio constant to within ± 2 per mil after 48 h. The plot shows the distribution at level four ($\sim$1 km) where the deviations are largest for this case. The budget calculations show that the mass is conserved to within five significant digits, using 32-bit arithmetics. These conservation properties are of major importance when simulating the distribution of long-lived trace species like CO_2 where accuracy in simulated variations in the mixing ratio of less than 1% is required.

b. Zero initial distribution and constant upper boundary

The importance of the adjustment of the wind field described in section 3 is illustrated in Figs. 4 and 5. Figure 4 shows the result from a 48-h simulation of a passive tracer where the model was initialized with a zero mixing ratio. A mixing ratio of 1000 ppt(m) was specified at the top of the model and kept constant throughout the simulation. The meteorological data were the same as in the simulation described above. Figure 4a shows the result when using unadjusted wind fields and no interpolation in time (i.e., the meteorological fields are kept constant for 6 h between updates). The inflow is confined to the top layers reaching down to 11 km, which appears quite realistic. Figure 4b shows a similar simulation, but in this case the meteorological data from HIRLAM has been interpolated in time to 1-h resolution within MATCH. No adjustment has been applied. Depending on location, the penetration of the inflow from the upper boundary varies. It reaches all the way down to about 1 km in one location connected to a trough region (cf. Fig 3). This is clearly unrealistic since the upper boundary is located well into the stratosphere. The corresponding results with adjusted wind fields are shown in Fig. 4c. Here the penetration is much more limited and appears almost comparable to the case without time interpolation and without adjustment. However, the penetration is still somewhat too deep, which indicates that the adjustment algorithm does not satisfy a full balance between mass and wind field. The penetration in Fig. 4a reaches the most realistic level, but keeping the meteorology constant in 6-h intervals may lead to other errors in simulation of transport, as discussed below.

Figure 5 shows a similar simulation but now based on data from the ECMWF global model for the same period and almost the same geographical domain as above. The meteorological fields have in this case been interpolated from spectral space (T213) to a 0.5° latitude $\times$ 0.5° longitude representation. The number of levels in the vertical is 31. Figure 5a shows the result when using unadjusted wind fields without time interpolation and where new meteorological data are available in 6-h intervals. The penetration is substantial reaching down to about 4.5 km, which is clearly unrealistic. When time interpolation is introduced to yield 1-h updates of weather data, Fig. 5b, the result is even worse. As when using data from HIRLAM the penetration depends on location. Locally it reaches down almost to the surface. The corresponding results with adjusted wind fields are shown in Fig. 5c. Here the penetration is much more limited and also more limited than when using data from HIRLAM. The inflow is confined totally to the top four layers in the model, which are all in the stratosphere. The difference compared to HIRLAM (Fig. 4c) is probably due to higher vertical resolution, which gives less numerical diffusion in the vertical advection, as calculated using an upstream scheme and a time-step of 300 s for both datasets.

The simulations summarized in Figs. 4 and 5 demonstrate the importance of ensuring that the wind field is in proper balance before use in an offline transport model. The need for adjustment varies depending on the quality of the meteorological data. Using model output from HIRLAM without temporal interpolation seems to give good results, indicating that the HIRLAM model output is well balanced. However, if time interpolation is used, the interpolated wind fields have to be adjusted. An alternative approach is, of course, to store data from the NWP model more frequently. The importance of the temporal resolution has been highlighted by Cats et al. (1987), who applied a trajectory model to the Chernobyl case with different update frequencies of input weather data. Cats et al. conclude that a time resolution of 1 h is comparable with an "online" model. Horizontal interpolation also deteriorates the balance as in the ECMWF case. Before using meteorological data from a spectral model adjustment is clearly necessary.

c. Simulation of release from a point source

As a final illustration of the performance of the model, simulations for a point source have been conducted. The

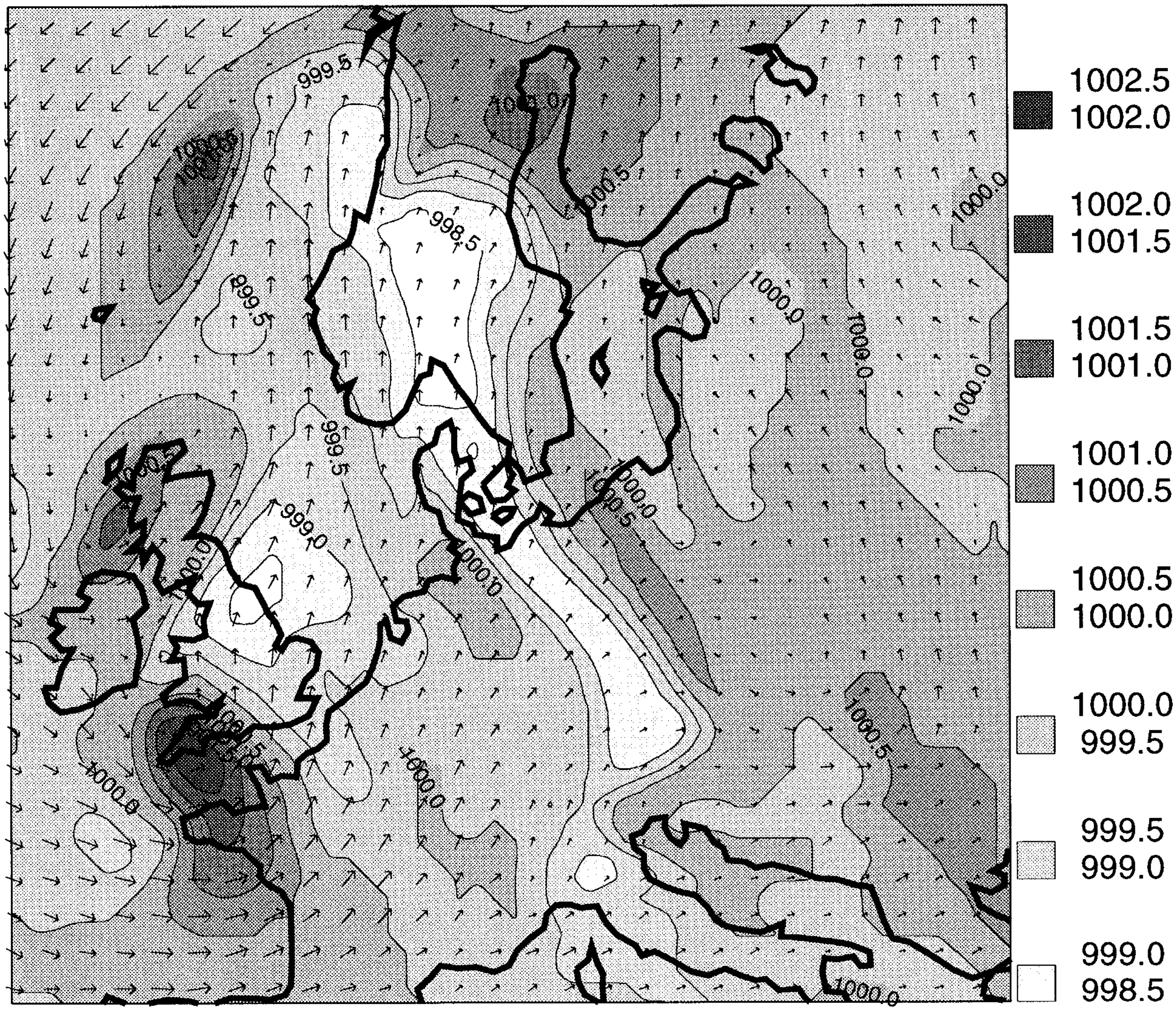

FIG. 3. Calculated distribution of a passive tracer after 48 h of simulation starting from constant distribution of 1000 ppt(m) and with constant boundary values of 1000 ppt(m). The plot refers to layer 4, i.e., ~1 km above ground. The meteorological data is from 1200 UTC 23 October 1994 to 1200 UTC 25 October 1994.

scenario has been taken from the ETEX-I tracer experiment (Graziani and Klug 1997). The ETEX dataset (Nodop et al. 1997) is very useful in this respect since it provides a well-known source function and observations with high temporal resolution at a large number of surface stations. However, given that an inert, nondepositing tracer was used, the ETEX experiment just facilitates evaluation of model performance in terms of advection and vertical diffusion.

Figures 6 and 7 show the evolution of the ETEX-I 12-h release from a surface point source located at 48°N, 2°W. Together with the 3-h concentrations, observations and near–surface winds are presented. The observations are shaded in the same shading scale as the calculations. Meteorological data are taken from HIRLAM, and the period is the same as in the simulations discussed above. Figure 6 shows the results when using the fifth-order integral flux scheme in the horizontal advection. The model is able to maintain sharp gradients in the distribution of the tracer in good agreement with the observations. This is clearly in contrast to the results shown in Fig. 7 where an upstream scheme has been used in the horizontal advection. In this case strong numerical diffusion is obvious, and the distribution is very flat 24 h after the release. The mass is conserved in both simulations as well as the positiveness of the distribution. These simulations clearly demonstrate the importance of using higher-order schemes for tracer advection.

It should be noted that proper handling of point sources demands an initialization process to account for the subgrid scale transport, during the initial phase of a point source release, before the cloud has reached a scale resolvable by the Eulerian model. The initialization problem of point sources will be addressed in a

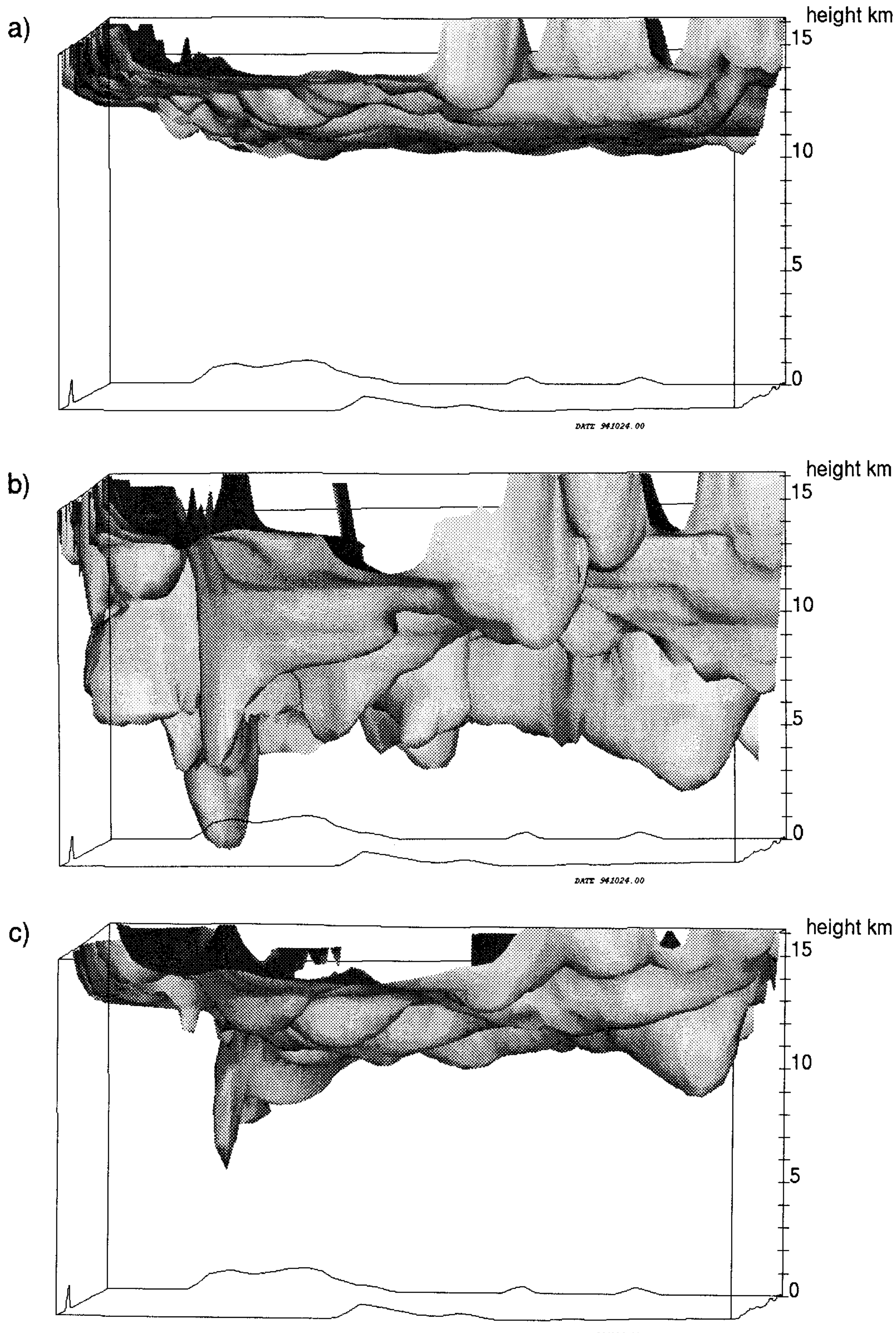

FIG. 4. Calculated penetration of a passive tracer from the top of the model domain, after 48 h of simulation, starting from a zero initial distribution using meteorological data from HIRLAM, as viewed from a location slightly below and to the left of the model domain. (a) No adjustment, no time interpolation; (b) no adjustment, time interpolation; and (c) with adjustment and time interpolation. Isosurface for 10 ppt(m). The mixing ratio at the upper boundary was fixed at 1000 ppt(m).

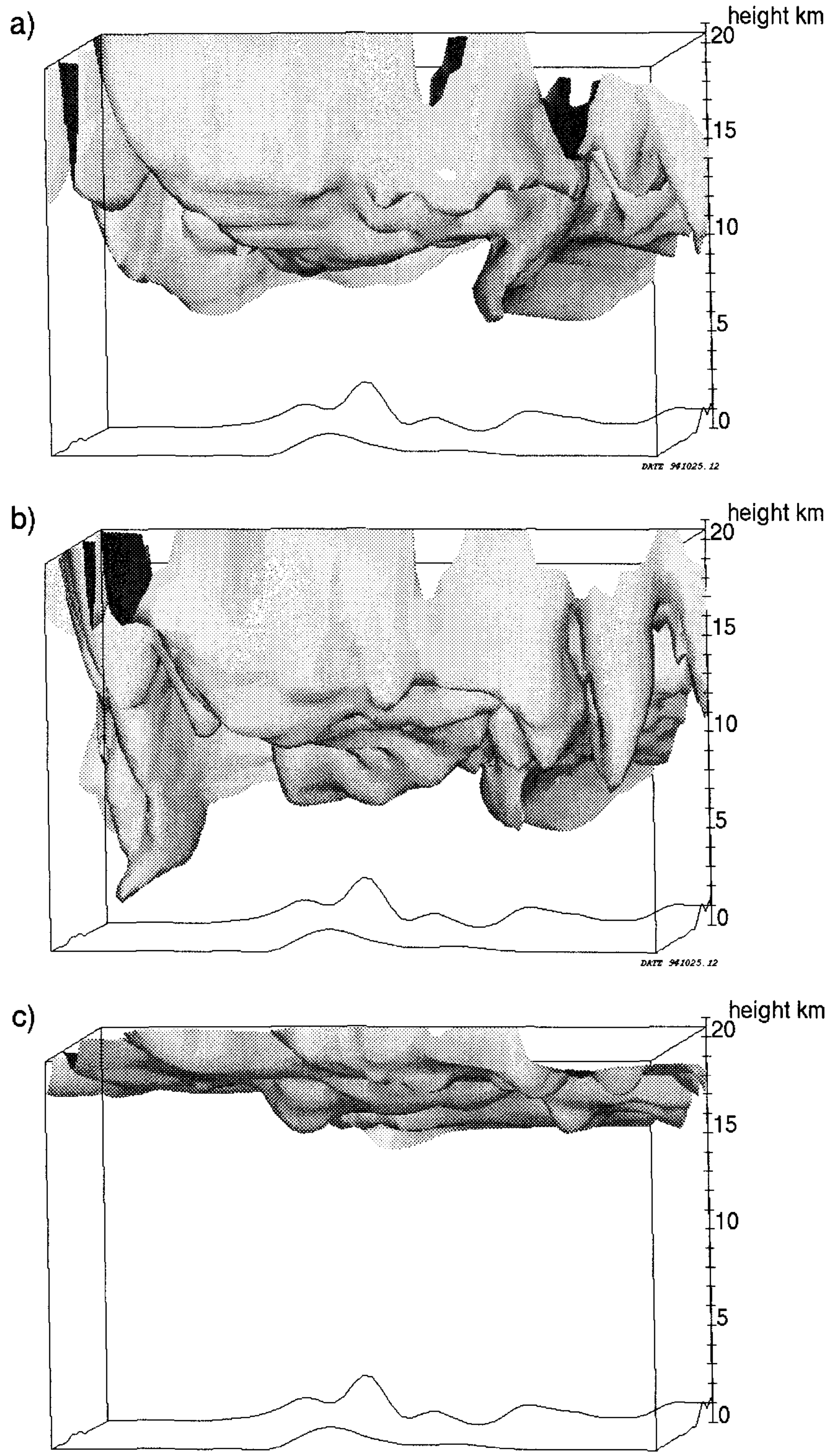

FIG. 5. Calculated penetration of a passive tracer from the top of the model domain, after 48 h of simulation, starting from a zero initial distribution using meteorological data from ECMWF, as viewed from a location slightly below and to the left of the model domain. (a) No adjustment, no time interpolation; (b) no adjustment, time interpolation; and (c) with adjustment and time interpolation. Isosurface for 10 ppt(m). The mixing ratio at the upper boundary was fixed at 1000 ppt(m).

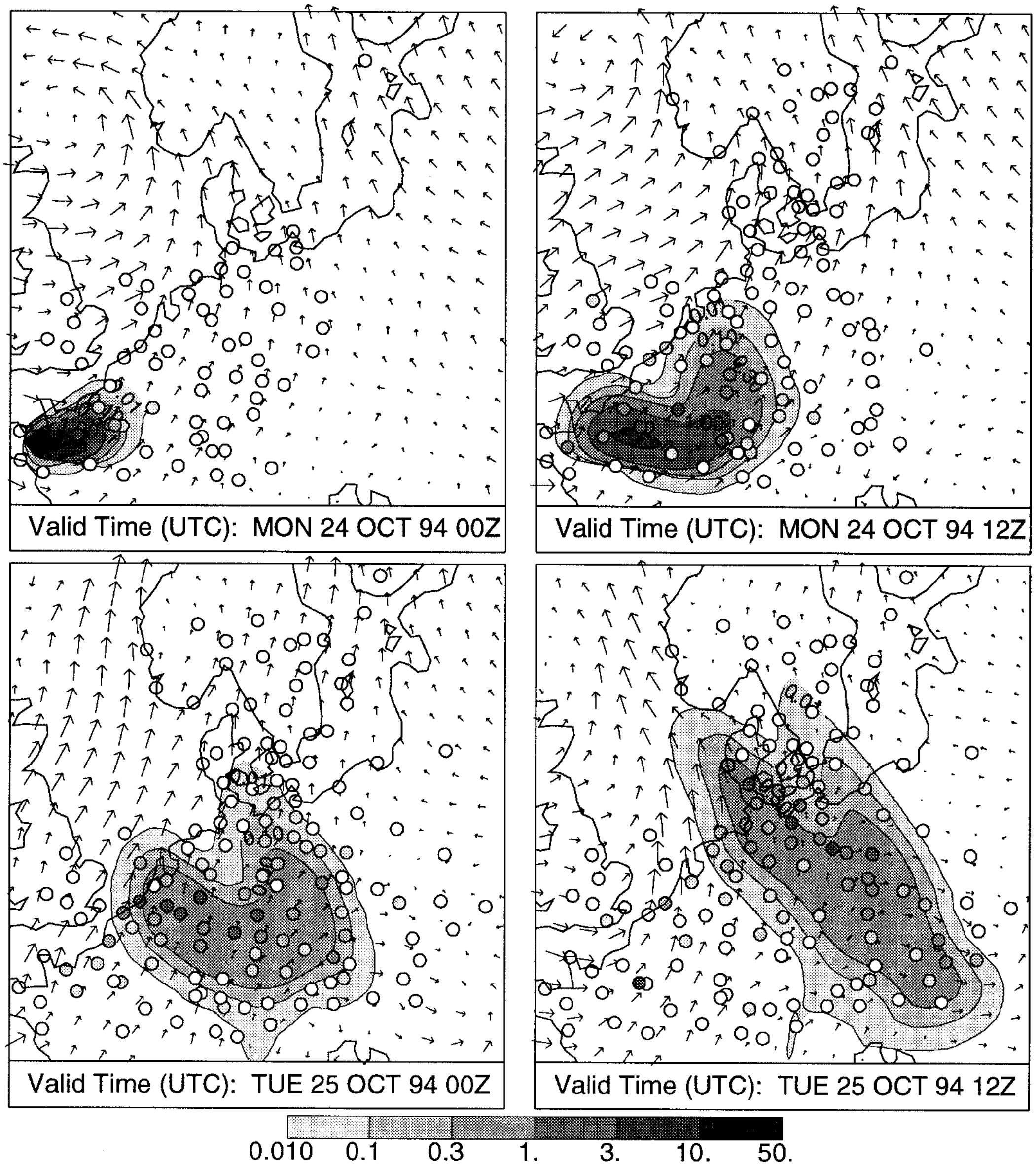

FIG. 6. Calculated distribution of a passive tracer released from a surface point source (ETEX-I) using a fifth-order scheme in the horizontal advection. The release starts at 1600 UTC 23 October 1994 and stops 12 h later. Resulting 3-h surface concentration after 12 (upper left), 24 (upper right), 36 (lower left), and 48 (lower right) h of simulation, together with observations and near-surface wind. The observation values are marked with the same shading as the simulation. Empty circles indicate verified zero measurements. Units in ng m^{-3}.

later publication. In the above simulations no such initialization was included, which means that the numerical diffusion is enhanced in the early phase of the release.

5. Control experiment with ^{222}Rn

Radon-222 is produced through the decay of ^{226}Ra and released to the atmosphere mainly from unglaciated surfaces of the earth. The ^{222}Rn flux from a unit area of the ocean is two orders of magnitude less than the corresponding terrestrial flux (Broecker et al. 1967; Wilkening and Clements 1975). Radon-222 decays with a half-life of 3.8 days, which makes it a potentially suitable tracer to investigate horizontal and vertical transport in the lower atmosphere, providing there are accurate measurements to compare with and that the emissions from a certain land area can be correctly determined. Such data are generally not available due to large natural variations in ^{222}Rn flux and atmospheric concentrations and an overall lack of observations. Keeping in mind the large uncertainties connected to ^{222}Rn emis-

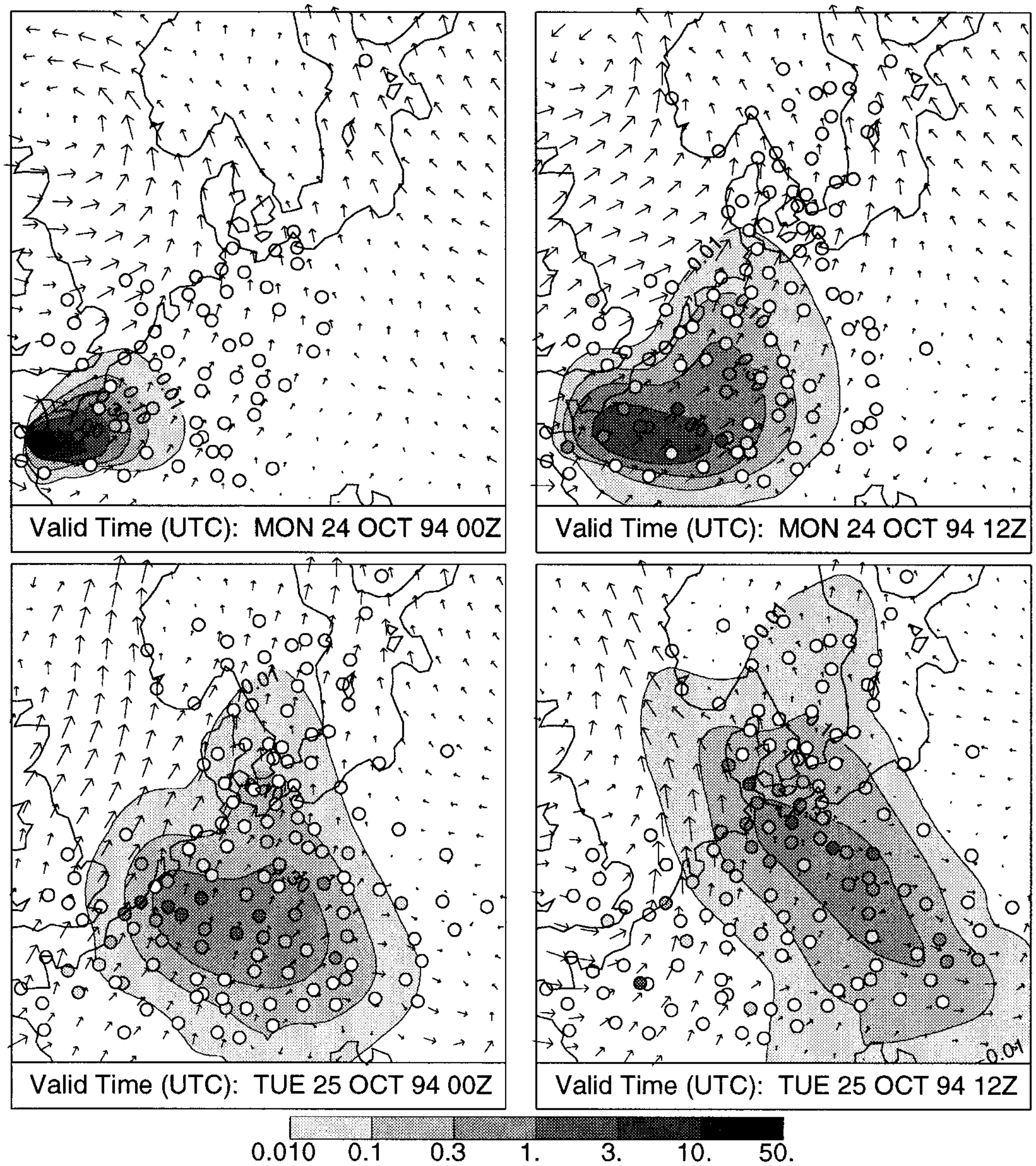

FIG. 7. Calculated distribution of a passive tracer released from a surface point source (ETEX-I) using an upstream scheme in the horizontal advection. The release starts at 1600 UTC 23 October 1994 and stops 12 h later. Resulting 3-h surface concentration after 12 (upper left), 24 (upper right), 36 (lower left), and 48 (lower right) h of simulation, together with observations and near-surface wind. The observation values are marked with the same shading as the simulation. Empty circles indicate verified zero measurements. Same units as in Fig. 6.

sion estimates, and the poorly known horizontal and vertical distribution of atmospheric ^{222}Rn, we will now follow other modelers and utilize ^{222}Rn as a semirealistic atmospheric tracer in MATCH. A special problem related to regional models is the question of assigning correct boundary data. It has previously been pointed out (see, e.g., Brost 1988) that above a few kilometers height, the uncertainty in the model result is mainly caused by the assigned tracer concentration on the lateral boundaries. At this stage, we do not want to introduce the extra uncertainty arising from specifying boundary values. Our goal is not to present a refined distribution of ^{222}Rn activity in the atmosphere but rather to demonstrate the performance of MATCH during different seasons.

To validate a transport model and its parameterizations of the vertical flux, measured and simulated ^{222}Rn time series and profiles should preferably coincide in time and space. This is especially true for MATCH since it is driven by ‘‘observed’’ meteorology and has a resolution that resolves the synoptic scale. Such data are, unfortunately, not available for this study. In the following we will instead compare instantaneous, and monthly mean, model results with typical ^{222}Rn measurements at different locations. Our results will also be compared with published studies using global three-dimensional transport models.

a. Source and decay terms

The amount of ^{222}Rn released from a unit surface of the earth is highly variable, and contradictory estimates appear in the literature. The flux depends on a number of factors in the soil and on atmospheric conditions. The most important factor, apart from the ^{226}Ra content of the crustal material, appears to be the soil porosity, which is often dependent on soil moisture, and the possible inhibiting of the flux by overlying snow and ice.

Due to the uncertainty in the quantification of the terrestrial–atmospheric flux of ^{222}Rn, we have, in the following, assigned all land surfaces south of 75°N a constant and uniform source of ^{222}Rn with the magnitude of 1.0 atom per centimeters squared per second, which is a value typically used by other modelers [see, e.g., Lin et al. (1996) and references therein]. Grid squares of Greenland and the Canadian Arctic, with an elevation of more than 300 m above sea surface, are assumed to be glaciated and consequently without ^{222}Rn flux to the atmosphere. Emissions from snow-covered land are not reduced. In addition, the soil freezing or possible differences in soil moisture are not taken into account in the current study. The ^{222}Rn emission is regarded as a nonbuoyant surface source and introduced into the lowest model layer prior to activating the advection modules.

The radioactive decay is calculated after advection and is described by an explicit formulation:

$$\mu^{t+\Delta t} = \mu^t - \lambda\mu^t\Delta t, \tag{23}$$

where λ is the decay constant for ^{222}Rn (2.097×10^{-6} s^{-1}).

b. Model setup

The following calculations are performed using meteorological data from the T213 global weather prediction model of ECMWF. Initialized analyses with 6-h temporal resolution are interpolated to a rotated latitude–longitude grid with $1° \times 1°$ horizontal resolution. The meteorological data are interpolated to 1-h temporal resolution with the adjustment procedure mentioned in section 3 applied. The internal time step is 300 s (for advection, vertical diffusion, and radioactive decay, respectively). The model atmosphere is divided into 31 unequally thick layers (cf. Fig. 12). The model domain is initialized with zero ^{222}Rn activity, and all boundaries set to zero throughout the integrations in order to isolate the performance of MATCH from the uncertainties arising from any specified boundary values.

Two ECMWF datasets are utilized. The first one is from 15 May to 30 June 1994, which represents spring and summer conditions. The second one is from 10 January to 28 February 1993, which represents winter conditions. Cloud cover, snow depth, and albedo, which are used to calculate the boundary layer parameters, are not available in the second dataset and have to be prescribed ad hoc. The total cloud cover is set to 4/8 over the entire area during the winter simulations. Sensitivity tests with various cloud covers show only a marginal impact on the results, and we therefore regard the results to be uncorrupted by this crude treatment of the cloud cover. Snow cover is assigned to grid cells in which the temperature in the lowest model layer is below −5°C. The albedo is given by predefined values for various surface types as shown in Table 1. The snowcover parameterization and albedo values are adopted without further sensitivity tests. In the spring–summer experiment the boundary layer height is constrained to never exceed 2.5 km; in winter it is constrained to 1 km.

TABLE 1. Predefined albedos for different surface types used to supplement the winter dataset.

Surface type	Albedo
Sea	0.5
Land	0.15
Snow	0.8
Ice	0.75

c. Comparison with measurements: Spring/summer

Figure 8 shows the calculated boundary layer height, z_{PBL}, and ^{222}Rn activity over two continental locations and one monitoring station in the Arctic for May and June 1994. Over central Europe (50°N, 10°E), MATCH calculates an atmospheric boundary layer that undergoes substantial diurnal variation. The ^{222}Rn activity near the surface is typically a factor of 2 higher during the morning hours as compared to the local afternoon when the boundary layer depth is the greatest. The results are very similar to measurements in Germany during August and September (Dörr et al. 1983) and in the eastern United States during summer (Jacob and Prather 1990). At layer 5 (~1 km) ^{222}Rn undergoes similar temporal variations as close to the surface, but the magnitude of the activity is lower.

Northern Siberia (70°N, 110°E) is probably still snow covered during this time of the year, and the atmospheric boundary layer is thus shallow. The diurnal surface temperature variation is also small, and there is only occasionally any diurnal variation of z_{PBL} and ^{222}Rn activity. Day-to-day variations in boundary layer height are often seen and a shallow boundary layer during several days results in higher ^{222}Rn near the surface, whereas a deep boundary layer results in lower ^{222}Rn near the surface. On occasions the simulations show more ^{222}Rn in layer 5 than near the surface. This must be caused by

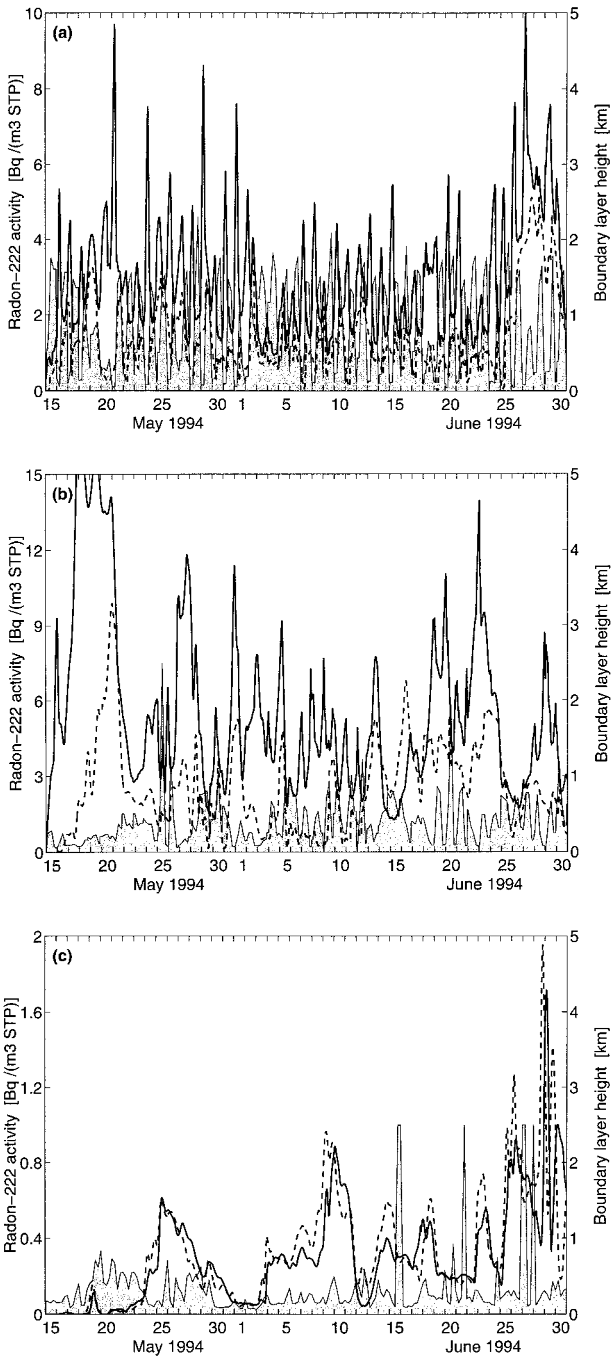

FIG. 8. Calculated boundary layer height z_{PBL} and ^{222}Rn activity for a summer period at three locations: (a) central Europe (50°N, 10°E), (b) northern Siberia (70°N, 110°E), and (c) Canadian Arctic (82°N, 62°W). Gray shading indicates boundary layer depth in kilometers; the thin solid line is the instantaneous ^{222}Rn activity every 1 h at the lowest model layer and the dashed line is the corresponding ^{222}Rn activity at model layer 5. Note the different scales in the three panels.

efficient vertical mixing at a location upwind and subsequent upper-air transport.

The calculated boundary layer height at the Arctic station (82°N, 62°W) is most often below 0.5 km without any diurnal variation. Since we have not specified any ^{222}Rn emissions near this site, changes in the local boundary layer is not affecting the ^{222}Rn activity and the ^{222}Rn activity in layers 1 and 5 are almost identical. The peaks in ^{222}Rn are connected to long-range transport from the source regions in Eurasia. Assuming a mean ^{222}Rn activity of 5 Bq m^{-3} (STP), normalized to standard pressure and temperature, in layers 1–5 over northern Siberia (see Fig. 9a), the ^{222}Rn events [reaching 1–2 Bq m^{-3} (STP)] correspond to a cross-polar transport of 5–10 days.

Figure 9 shows average ^{222}Rn activity for June 1994 in model layers 1 (0–60 m) and 15 (~6 km above surface). The simulated monthly mean ^{222}Rn activity in the lowest model layer is typically 4–5 Bq m^{-3} (STP) over the continents. Maximum monthly mean values occur in northeastern Siberia and reach 7 Bq m^{-3} (STP). Over the Arctic and the oceanic regions, monthly mean ^{222}Rn activity is below 1 Bq m^{-3} (STP). Lambert et al. (1982) estimate the annual mean ^{222}Rn activity to be 4.6 Bq m^{-3} (STP) over the Northern Hemisphere (NH) continents and 0.2 Bq m^{-3} (STP) over the NH oceans. Larson et al. (1972) report values around 0.1 Bq m^{-3} (STP) from ship measurements in the Greenland and Norwegian Sea during August. Leck et al. (1996) measured ^{222}Rn in the ice-covered Arctic and in the Fram Strait in August and September; their data range from 0.01 to 0.6 Bq m^{-3} (STP). In a short dataset from the Zeppelinfjellet monitoring station on Spitsbergen (79°N, 12°E), Lehrer et al. (1997) report ^{222}Rn background activities of 0.08 Bq m^{-3} (STP) with pulses reaching 0.5 Bq m^{-3} during the spring of 1995 and 1996. At model layer 15 (~6 km) large regions have ^{222}Rn activities in excess of 0.1 Bq m^{-3} (STP), and maximum values reach 0.4 Bq m^{-3} (STP).

d. Comparison with measurements: Winter

To unambiguously distinguish the behavior of our chosen atmospheric boundary layer parameterizations we have deliberately used the same surface emissions of ^{222}Rn during winter as during summer. This will probably result in too high ^{222}Rn activity in the model during winter, especially at high latitudes, where the flux to the atmosphere may be inhibited by overlying snow and frozen soil.

Figure 10 shows the temporal evolution of the calculated boundary layer height and ^{222}Rn activity in January and February 1993. In winter, the calculated continental boundary layer over central Europe (50°N, 10°E) is shallow and displays no diurnal variation. The modeled changes in ^{222}Rn activity at this site are primarily due to day-to-day variations in the depth of the local boundary layer. The ^{222}Rn activities are generally larger near the surface in winter than in summer, and the difference between layers 1 and 5 is also much greater in winter than in summer (cf. Fig. 8a). The same

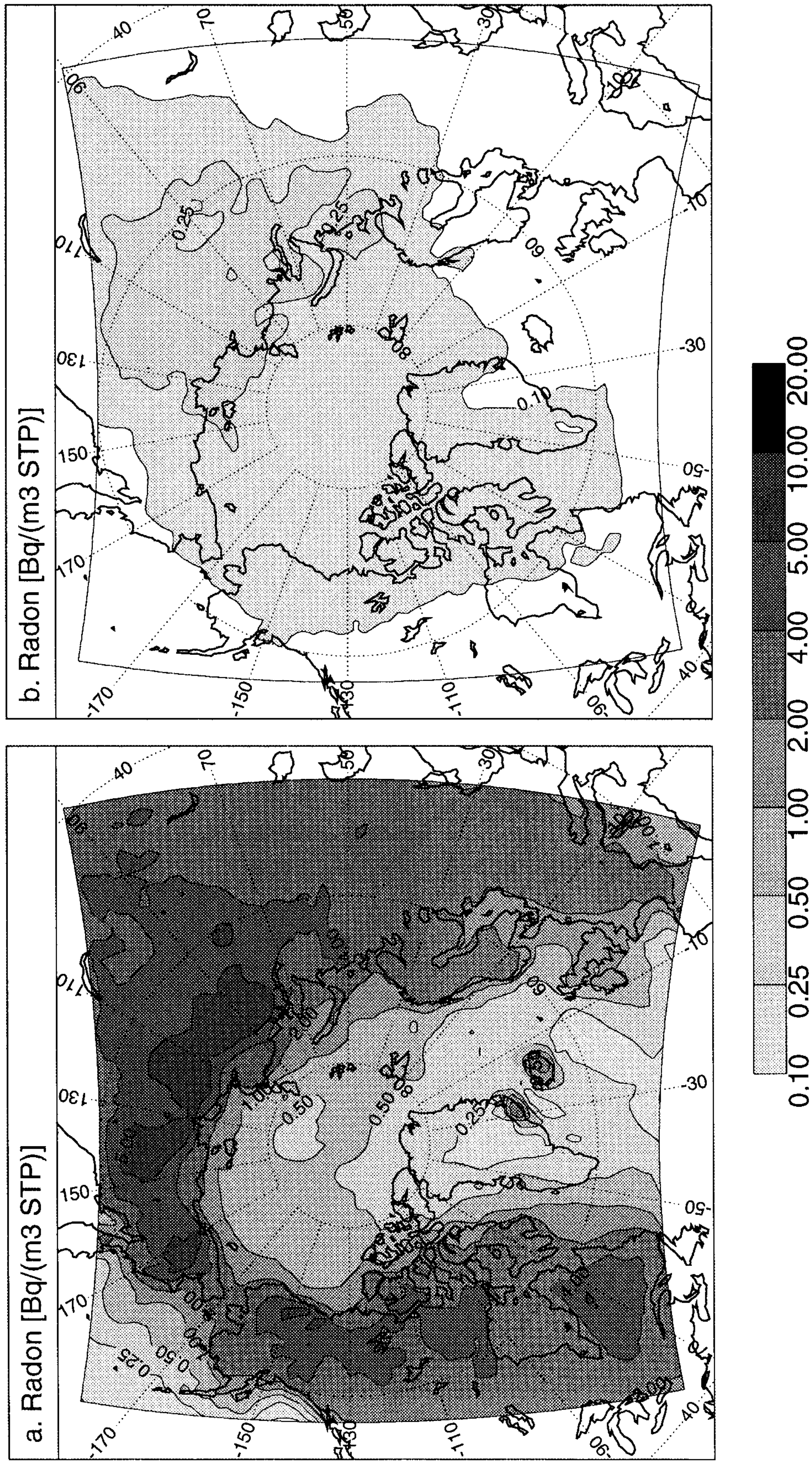

FIG. 9. Mean horizontal distribution of ^{222}Rn for spring and summer and for lowest model layer (left) and layer 15, 6.5 km above ground, (right). Units Bq m^{-3} (STP).

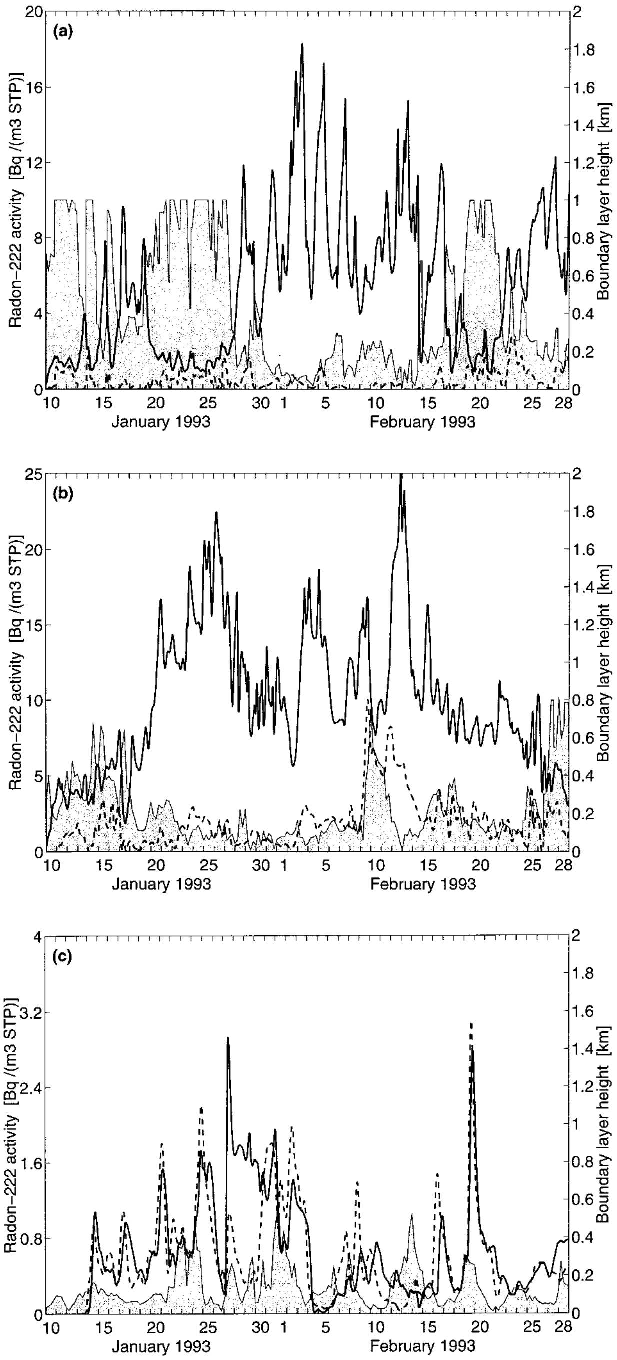

FIG. 10. Calculated boundary layer height z_{PBL} and ^{222}Rn activity for a winter period at three locations: (a) central Europe (50°N, 10°E), (b) northern Siberia (70°N, 110°E), and (c) Canadian Arctic (82°N, 62°W). Gray shading indicates boundary layer depth in kilometers; the thin solid line is the instantaneous ^{222}Rn activity every 1 h at the lowest model layer and the dashed line is the corresponding ^{222}Rn activity at model layer 5. Note the different scales in the three panels.

features are even more prominent at the Siberian site (70°N, 110°E) due to an even shallower boundary layer.

In locations downwind of the continental source regions [exemplified by the Arctic site (82°N, 62°W) in Fig. 10c], high ^{222}Rn activities are occasionally seen as pulses with distinct start and stop times. The absolute values and the shape of the peaks are similar to what Worthy et al. (1994) reported for Alert (82°N, 62°W) in February 1992 (0.5–3 Bq m^{-3} STP).

Figure 11 shows average ^{222}Rn activity in model layers 1 (0–60 m) and 15 (~6 km) for February 1993. Over the emission regions the monthly mean surface values are typically greater than 5 Bq m^{-3} (STP) with maximum monthly mean values reaching almost 15 Bq m^{-3} (STP). When comparing with summer conditions (Fig. 9) it is obvious that the winter surface ^{222}Rn activity is larger, both over the emission regions and in the ice-covered Arctic. Jacob and Prather (1990) reviewed measurements performed in the U.S. and showed that the monthly mean ^{222}Rn activity near the surface in winter was roughly a factor of 2 greater than in summer [8 and 4 Bq m^{-3} (STP), respectively]. Similar features were reported for Europe by Feichter and Crutzen (1990), who review data from Freiburg, Germany. The near–surface monthly mean ^{222}Rn activity in Freiburg had a maxima in November and a minima in March–May [7 and 3 Bq m^{-3} (STP), respectively]. At model layer 15 (~6 km) the activity is significantly lower during winter than summer, which is attributed to the much less efficient vertical mixing then. Maximum average values barely reach 0.2 Bq m^{-3} (STP).

A problem in these analyses is the assigned open boundaries. All inflow to the domain will dilute the mixing ratios of ^{222}Rn. This is, for example, apparent in a wedge over the Atlantic where southwesterly winds bring radon-free air into the domain both during the summer and winter (see Figs. 9 and 11). The boundary effect becomes increasingly dominant at higher altitudes, and at 6 km the results are almost entirely determined by the boundary values (Lin et al. 1996).

e. Mean vertical distribution

In Fig. 12 we show monthly mean vertical profiles of ^{222}Rn activity in MATCH for June 1994 and February 1993 over the three sites discussed above. It is clear that the vertical mixing in MATCH is greater in summer than in winter, a feature that is also seen in the measurements of ^{222}Rn. The timescale for transport from the boundaries to the interior of the domain is less than for transport from the surface to the upper layers of the model. Our profiles and the Liu et al. (1984) data are therefore strictly not comparable, and the discrepancy will increase the higher up in the domain one gets. Naturally, the difference decreases farther from the boundaries of MATCH, as indicated by the better correspondence between MATCH and Liu et al. for the Siberian site (Fig. 12b), as compared to the European site (Fig.

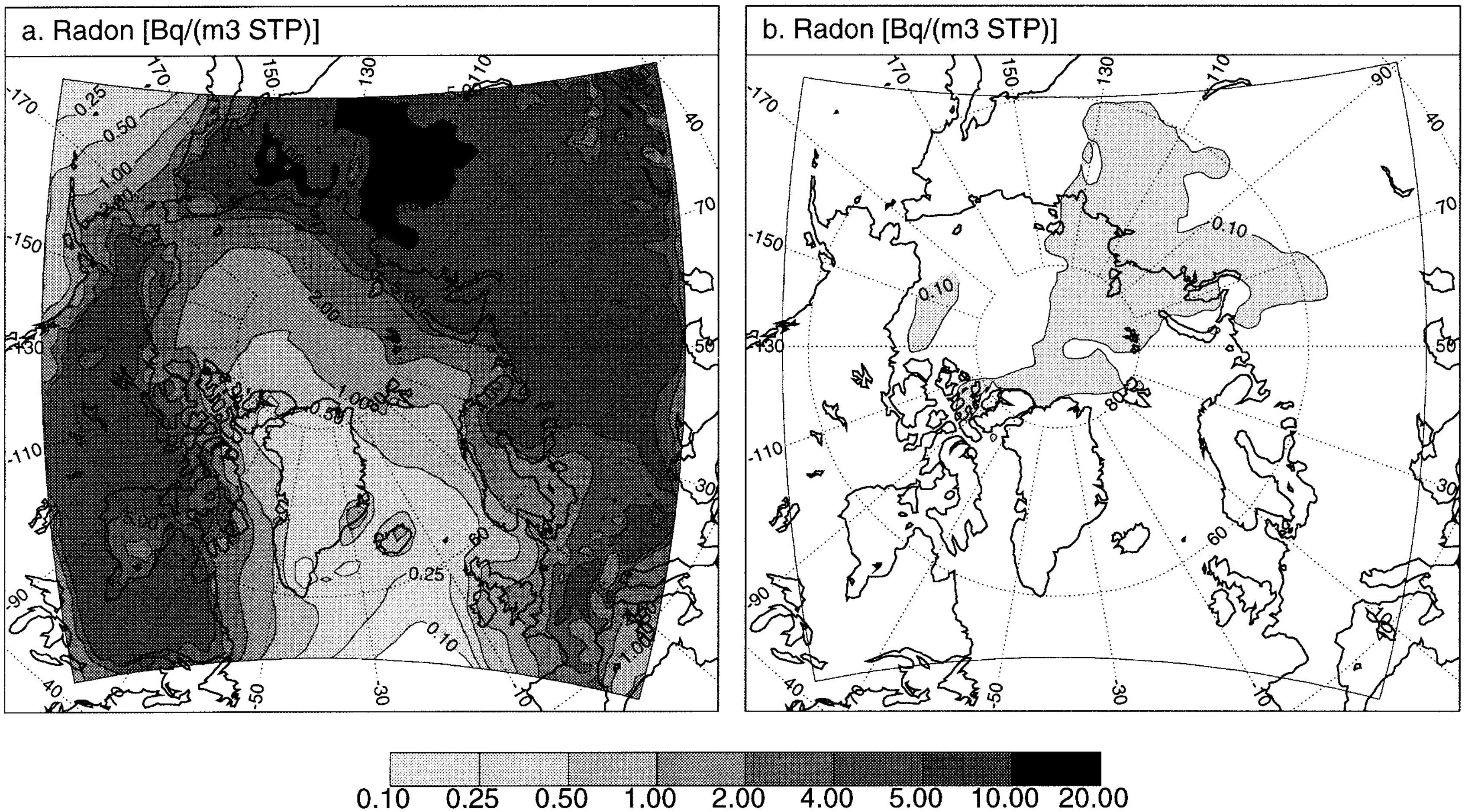

FIG. 11. Mean horizontal distribution of ^{222}Rn for a winter period and for lowest model layer (left) and layer 15, 6.5 km above ground, (right). Units in Bq m^{-3} (STP).

12a). It should also be noted that the Liu et al. data are a compilation of only 23 profiles in summer and 7 profiles in winter and that the uncertainty in the data is considerable due to the natural variations in ^{222}Rn activity.

Moore et al. (1977) found ^{222}Rn activities of 0.4 Bq m^{-3} (STP) from the surface up to the tropopause in the eastern Pacific. The lack of negative vertical gradient over oceanic regions was also confirmed by Andreae et al. (1988), who reported constant [0.2 Bq m^{-3} (STP)], or increasing ^{222}Rn activity off the coast of Washington, and by Ramonet et al. (1996), who often found higher ^{222}Rn at a few kilometers than near the surface of the Atlantic. Wilkniss and Larson (1984) concluded from several years of data in the Arctic that the boundary layer values were typically below 0.5 Bq m^{-3} (STP). Due to a more efficient transport in the free troposphere than near the surface, they also often noted similar or higher values aloft. As shown in Fig. 12c, MATCH simulates similar, constant tropospheric ^{222}Rn activity during summer at a remote Arctic site. During winter, the increased stability over the emission regions is apparent as a monotone decrease of ^{222}Rn above the lowest few layers of the Arctic site.

f. Comparison with other models

Although we have limited measured data for comparison, other model results can be used as an additional source of information. Global models typically calculate a slightly higher ^{222}Rn activity near the surface for NH continents during winter than in summer due to less effective mixing in winter. The few exceptions that appear arise from the formulation of the source function, for example, suppressed emissions during soil freezing or snow cover.

Genthon and Armengaud (1995) present near-surface, annual mean ^{222}Rn activities over Eurasia and Northern America. Their values lie between 2 and 4 Bq m^{-3} (STP). Feichter and Crutzen (1990), Heimann and Feichter (1990), and Balkanski et al. (1993) typically allocate the near-surface grid squares of Eurasian, ^{222}Rn activities of 2–5 Bq m^{-3} (STP) in summer and 2–10 Bq m^{-3} (STP) in winter. The values are slightly lower than ours, which we ascribe to the coarser vertical resolution in these models.

Feichter and Crutzen (1990) and Balkanski et al. (1993) simulate ^{222}Rn activity over Eurasia and Northern America at 500 hPa and 6 km, respectively, to be 0.1–0.2 Bq m^{-3} (STP) in January. Balkanski et al. (1993) also give the corresponding values for July, which are more than twice as high as their winter values. The midtropospheric ^{222}Rn values of the global models are generally higher than in MATCH (cf. Figs. 9b, 11b), which is a consequence of our assigned open boundaries, which will dilute all ^{222}Rn mixing ratios in the interior of the domain.

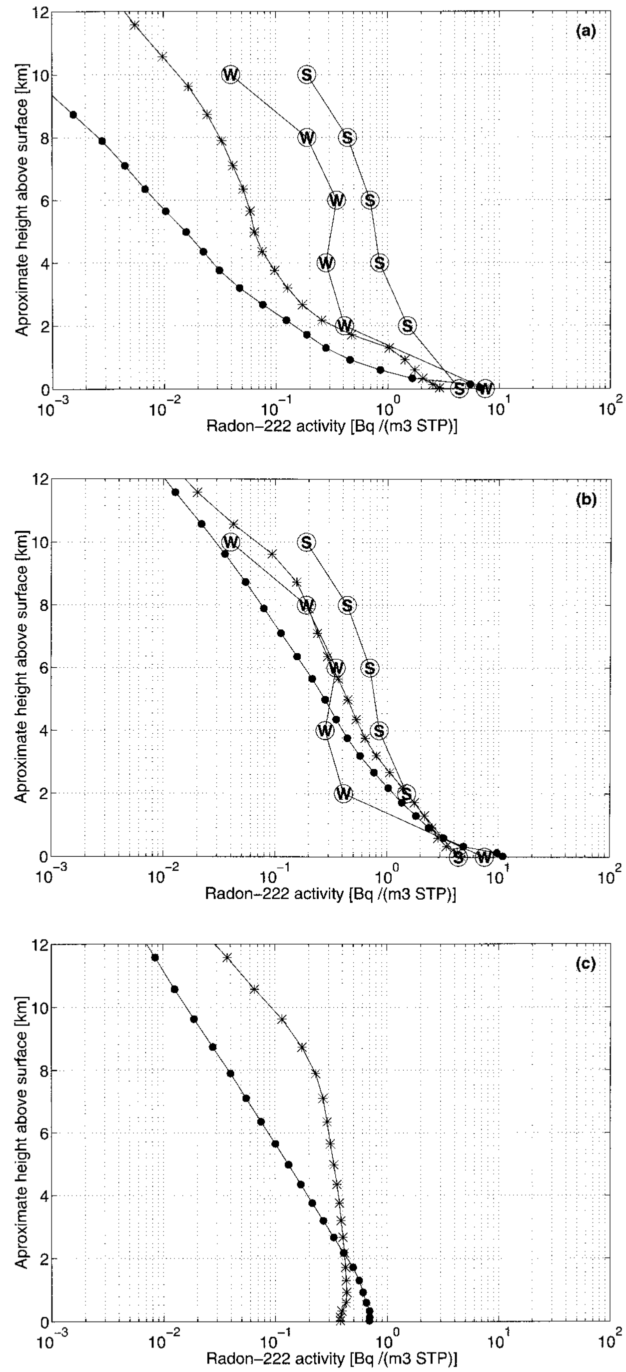

FIG. 12. Simulated mean summer (asterisks) and winter (dots) vertical profiles of ^{222}Rn activity for three locations: (a) central Europe (50°N, 10°E), (b) northern Siberia (70°N, 110°E), and (c) Canadian Arctic (82°N, 62°W). In (a) and (b) are also shown average continental profiles for summer (S) and winter (W), as reviewed by Liu et al. 1984.

g. Summary of ^{222}Rn simulations

Using the radioactive tracer ^{222}Rn, we have demonstrated some characteristics of the MATCH transport model.

In sections 5c and 5d we showed that the calculated continental boundary layer undergoes substantial diurnal variation in summer. Due to the increased stability in winter, the parameterized vertical mixing is then smaller and the resulting ^{222}Rn activity close to the ground larger, compared to summer conditions, all in accordance with observations. The near-surface ^{222}Rn time series and average horizontal distributions for summer and winter are very similar to published measurements, both for the continental regions and the more remote, oceanic and Arctic sites.

In section 5e we demonstrated that the vertical gradient of ^{222}Rn is very pronounced over a continental site during winter and less so during summer. Over noncontinental regions the ^{222}Rn activity in the model's boundary layer, and the lower troposphere, is rather uniform, especially in summer, features that are all seen in measured data. At oceanic and Arctic sites, both the model and measurements occasionally show enhanced activity at a few kilometers height due to the more rapid horizontal transport there. Moreover, near-surface measurements at remote sites often reveal periods with relatively high ^{222}Rn activity. These episodes are characterized by distinct start and stop times although the emissions occurred several days ago. In sections 5c and 5d we showed that the advection scheme in MATCH was able to maintain sharp gradients in ^{222}Rn activity with only small diffusion over long periods.

The calculated vertical gradient of ^{222}Rn activity, discussed in sections 5e and 5f, is larger in MATCH than in global transport models, and it is probably also too large compared to measurements. This is, however, to be expected since in our experiments the boundaries were assigned zero ^{222}Rn and the transport time from the boundaries to a point in the middle of the model domain is smaller than the transport time from the surface up to the middle troposphere. The absence of parameterized deep convection may also contribute to the discrepancy.

In conclusion, although the available measurements permits only rough comparisons, we have demonstrated reasonable levels of ^{222}Rn activity in MATCH throughout the boundary layer. We have also shown realistic seasonal and spatial variations of ^{222}Rn in the lower troposphere. The only apparent discrepancy between our model and other studies can be attributed to the experimental design (i.e., the open boundaries) and the possible impact from convective transport in clouds not described in MATCH.

6. Conclusions

A limited-area, offline, Eulerian atmospheric transport model has been developed. The model is designed to be flexible with regard to horizontal and vertical domain and input meteorological data and provides a framework for application to a wide range of problems in atmospheric transport and chemistry modeling. Mass conservation and maintenance of a positive definite solution is obtained by formulating the equations in flux form. An optional adjustment module, which provides a balanced wind field, is implemented so that meteorological data from various sources can be utilized. This module makes it possible to also use time-interpolated meteorological input data if desired without loss of accuracy. The test simulations presented clearly demonstrates the ability of the model to meet a number of common requirements on an atmospheric transport model such as mass conservation, positive definiteness, maintenance of constant field, and shape preservation. The tests also demonstrates the importance of using balanced wind fields.

The simulations of ^{222}Rn indicates qualitatively the ability of the model to simulate a real atmospheric tracer, and some characteristics of the MATCH transport model are demonstrated. Although the available measurements only permit rough comparisons, we have demonstrated reasonable levels of ^{222}Rn activity in MATCH throughout the boundary layer. We have also shown realistic seasonal and spatial variations of ^{222}Rn in the lower troposphere. The only apparent discrepancy between our model and other studies can be attributed to the experimental design and the possible impact from convective transport in clouds not described in MATCH, which both should be addressed in forthcoming studies.

Acknowledgments. The MATCH transport model is a result of a continuous development over the last 5 years. This work was initiated by Christer Persson at SMHI, who also was a key person in the development of the first versions of MATCH. His continued support and expertise has been invaluable for the development of the present version. The implementation of η coordinates would not have been possible without the support from the HIRLAM group at SMHI. In particular we have benefited from discussions with Stefan Gollvik and Nils Gustafsson. We also thank Erland Källén, Hilding Sundqvist, Elias Hólm, and Stephen Craig at the Department of Meteorology, Stockholm University (MISU) for valuable discussions and finally Henning Rodhe and Kim Holmén for their constructive criticism and continued support. Special thanks go to Ulf Hansson at MISU for guiding one of us (M.E.) through the complicated world of FORTRAN programs and GRIB codes.

APPENDIX

Primitive Functions

The primitive function of the mass distribution is simply a spatial integral of the mass, defined over a certain interval,

$$Q(x, t) = \int_0^x q(x', t)\, dx' + C, \qquad \text{(A1)}$$

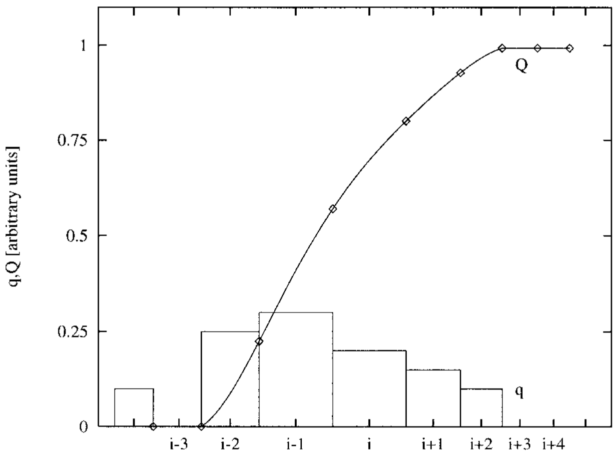

FIG. A1. An example of a discrete distribution q and its primitive function Q defined over the interval $i - 3$ to $i + 4$ (q and Q have different units). The diamonds denote the points where the primitive function is uniquely defined. Note the irregular grid spacing.

where C is an arbitrary constant that we chose to be zero. The interval could be any subdomain of the model area, and x refers to the coordinate within this interval. It is obvious that the primitive function is known exactly at the boundaries of each grid cell by summing up the known discrete masses up to each cell boundary,

$$Q_i(t) = \sum_{k=0}^{i} \tilde{q}_k(t)\Delta x_k, \tag{A2}$$

where $\tilde{q}$ is the discrete value and k is the "internal" index of the grid cells within the interval selected, and $Q_0 \equiv 0$. This generates a set of discrete integral values, $Q_0, Q_1, Q_2, \ldots,$ from which a continuous formula can be approximated by some fitting technique. Applying a Lagrangian polynomial fitting yields

$$Q(x, t) = \sum_{k=0}^{n} \alpha_k(x)Q_k(t), \tag{A3}$$

where the Lagrangian polynomial weights are defined by

$$\alpha_k(x) = \prod_{j=0,\ j\neq k}^{n} \frac{x - x_j}{x_j - x_k}. \tag{A4}$$

Here x_j represents the coordinates to the cell boundaries in the local coordinates of the interval, and $x_0 = 0$. Figure A1 shows the relation between a discrete distribution and its primitive function. The local value and local gradients may be derived by differentiation of the primitive function, thus

$$q(x, t) = \frac{\partial}{\partial x}Q(x, t) = \sum_{k=0}^{n} \frac{d}{dx}\alpha_k(x)Q_k(t) \tag{A5}$$

and

$$\frac{\partial}{\partial x}q(x, t) = \frac{\partial^2}{\partial x^2}Q(x, t) = \sum_{k=0}^{n} \frac{d^2}{dx^2}\alpha_k(x)Q_k(t). \tag{A6}$$

The instantaneous value could be derived in the same fashion by defining a primitive function in time. Note that the local value at the center point of a grid cell may not be equal to the discrete value in this cell.

REFERENCES

Andreae, M. O., H. Berresheim, T. W. Andreae, M. A. Kritz, T. S. Bates, and J. T. Merrill, 1988: Vertical distribution of dimethylsulfide, sulfur dioxide, aerosol ions, and radon over the northeast Pacific Ocean. *J. Atmos. Chem.,* **6,** 149–173.

Balkanski, Y. J., D. J. Jacob, G. M. Gardner, W. C. Graustein, and K. K. Turekian, 1993: Transport and residence times of tropospheric aerosols inferred from a global three-dimensional simulation of ^{210}Pb. *J. Geophys. Res.,* **98D,** 20 573–20 586.

Berkowicz, R., H. R. Olesen, and U. Torp, 1986: The Danish Gaussian air pollution model (OML): Description, test and sensitivity analysis in view of reglatory applications. *Proc. 15th NATO/CCMS Int. Technical Meeting on Air Pollution Modeling and Its Application,* St. Louis, MO, NATO/CCMS, 453–481.

Bott, A., 1989a: A positive definite advection scheme obtained by nonlinear renormalization of the advective fluxes. *Mon. Wea. Rev.,* **117,** 1006–1015.

——, 1989b: Reply. *Mon. Wea. Rev.,* **117,** 2633–2636.

——, 1992: Monotone flux limitation in the area-preserving flux-form advection algorithm. *Mon. Wea. Rev.,* **120,** 2592–2602.

Broecker, W. S., Y. H. Li, and J. Cromwell, 1967: Radium-226 and radon-222: Concentration in Atlantic and Pacific oceans. *Science,* **158,** 1307–1310.

Brost, R. A., 1988: The sensitivity to input parameters of atmospheric concentrations simulated by a regional chemical model. *J. Geophys. Res.,* **93D,** 2371–2387.

Burridge, D. M., and A. J. Gadd, 1977: The Meteorological Office operational 10-level numerical weather prediction model. Meteorological Office Sci. Paper 34, 39 pp. [Available from Meteorological Office, Bracknell, Berkshire RG12 2sz, England.]

Businger, J. A., J. C. Wyngaard, Y. Izumi, and E. F. Bradley, 1971: Flux profile relationships in the atmospheric surface layer. *J. Atmos. Sci.,* **28,** 181–189.

Carmichel, G. R., and L. K. Peters, 1984: An Eulerean transport/transformation/removal model for SO_2 and sulfate. I. Model development. *Atmos. Environ.,* **18,** 937–951.

Cats, G. J, B. J. de Haan, and L. M. Hafkenschied, 1987: Verification of an objective analysis scheme. Meteorological analyses after the Chernobyl disaster verified by trajectories of radioactive air masses. Royal Netherlands Meteorological Institute *Scientific Report* WR 87-4, 15 pp. [Available from Royal Netherlands Meteorological Institute, P.O. Box 201, NL-3730 AE de Bilt, the Netherlands.]

Chang, J. S., R. A. Brost, I. S. A. Isaksen, S. Madronich, P. Middleton, W. R. Stockwell, and C. J. Walcek, 1987: A three-dimensional Eulerian acid deposition model. Physical concept and model formulation. *J. Geophys. Res.,* **92,** 14 681–14 700.

Crowley, W. P., 1968: Numerical advection experiments. *Mon. Wea. Rev.,* **96,** 1–11.

Dörr, H., B. Kromer, I. Levin, K. O. Münich, and H.-J. Volpp, 1983: CO_2 and Radon 222 as tracers for atmospheric transport. *J. Geophys. Res,* **88C,** 1309–1313.

Ebel, A., H. Hass, H. J. Jakobs, M. Laube, M. Memmersheimer, A. Oberrede, H. Geiss, and Y.-H. K'uo, 1991: Simulation of ozone intrusion caused by a tropopause fold and cut-off low. *Atmos. Environ.,* **25A,** 2131–2144.

Feichter, J., and P. J. Crutzen, 1990: Parameterization of vertical tracer tranport due to deep cumulus convection in a global transport model and its evaluation with ^{222}Radon measurements. *Tellus,* **42B,** 100–117.

Genthon, C., and A. Armengaud, 1995: Radon 222 as a comparative tracer of transport and mixing in two general circulation models of the atmosphere, *J. Geophys. Res.,* **100D,** 2849–2866.

Graziani, G., and W. Klug, 1997: The European Long-Range Tracer Experiment ETEX: Evaluation of the model intercomparison. *Proc. ETEX Symp. on Long-Range Atmospheric Transport, Model Verification and Emergency Response,* Vienna, Austria, European Commission, 105–108.

Heimann, M., and C. D. Keeling, 1989: A three dimensional model of atmospheric CO_2 transport based on observed winds. 2. Model description and simulated tracer experiments. *Aspects of Climate Variability in the Pacific and the Western Americas,* D. H. Peterson, Ed., Amer. Geophys. Union, 237–275.

——, and J. Feichter, 1990: A comparison of three-dimensional atmospheric transport models by means of simulatioms of radon-222. Rep. 8, Meteorological Institute, University of Hamburg, Hamburg, Germany, 29 pp. [Available from Meteorological Institute, University of Hamburg, Bundesstr. 55, DE-2000 Hamburg 13, Germany.]

Hólm, E. V., 1995: A fully two-dimensional, nonoscillatory advection scheme for momentum and scalar transport equations. *Mon. Wea. Rev.,* **123,** 536–552.

Holtslag, A. A. M., E. van Meijgaard, and W. C. De Rooy, 1995: A comparison of boundary layer diffusion schemes in unstable conditions over land. *Bound.-Layer Meteor.,* **76,** 69–95.

Jacob, D. J., and M. J. Prather, 1990: Radon-222 as a test of convective transport in a general circulation model. *Tellus,* **42B,** 118–134.

Källén, E., 1996: HIRLAM documentation manual—System 2.5. 106 pp. [Available from SMHI, SE-601 76 Norrköping, Sweden.]

Lambert, G., G. Polian, J. Sanak, B. Ardouin, A. Buisson, A. Jegou, and J. C. Le Roulley, 1982: Radon and daughter products cycle. Application to troposphere–stratosphere exchanges (in French). *Ann. Geophys.,* **38,** 497–531.

Langner, J., and H. Rodhe, 1991: A global three-dimensional model of the troposphere sulfur cycle. *J. Atmos. Chem.,* **13,** 225–263.

——, C. Persson, and L. Robertson, 1995: Concentration and deposition of acidifying air pollutants over Sweden. Estimates for 1991 based on the MATCH model and observations. *Water, Air, Soil Pollut.,* **85,** 2021–2026.

——, ——, ——, and A. Ullerstig, 1996: Air pollution assessment study using the MATCH modelling system. Application to sulfur and nitrogen compounds over Sweden 1994. Swedish Meteorological and Hydrological Institute Reports Meteorology and Climatology 69, 26 pp. [Available from SMHI, SE-601 76 Norrköping, Sweden.]

Larson, R. E, R. A. Lamontagne, and P. E. Wilkniss, 1972: Radon-222, CO, CH_4 and continental dust over the Greenland and Norwegian Seas. *Nature,* **240,** 345–347.

Leck, C., E. K. Bigg, D. S. Covert, J. Heintzenberg, W. Maenhaut, E. D. Nilsson, and A. Wiedensohler, 1996: Overview of the atmospheric research program during the International Arctic Ocean Expedition of 1991 (IAOE-91) and its scientific results. *Tellus,* **48B,** 136–155.

Lehrer, E., U. Langendörfer, D. Wagenbach, and U. Platt, 1997: Tropospheric ozone depletion related air mass characteristics. *Atmospheric Research in Ny-Ålesund,* I. Flöisand et al., Eds., Norsk Institutt for Luftforskning, 127–130.

Lin, X., F. Zaucker, E.-Y. Hsie, M. Trainer, and S. A. McKeen, 1996: Radon 222 simulations as a test of a three-dimensional regional transport model. *J. Geophys. Res.,* **101D,** 29 165–29 177.

Liu, S. C., J. R. McAfee, and R. J. Cicerone, 1984: Radon-222 and tropospheric vertical transport. *J. Geophys. Res.,* **89D,** 7291–7297.

Moore, H. E., S. E. Poet, and E. A. Martell, 1977: Vertical profiles of ^{222}Rn and its long-lived daughters over the eastern Pacific. *Environ. Sci. Technol.,* **11,** 1207–1210.

Nodop, K., R. Connoly, and F. Girardi, 1997: The European Tracer Experiment—Experimental results and database. *Proc. ETEX Symp. on Long-Range Atmospheric Transport, Model Verification and Emergency Response,* Vienna, Austria, European Commission, 59–62.

Persson, C., L. Robertson, K. Häggkvist, and L. Meuller, 1990: Mesoskalig spridningsmodell—Modellanpassning till Skånergionen. Swedish Meteorological and Hydrological Institute, Rapport-Meteorologi, 45 pp. [Available from SMHI, SE-601 76 Norrköping, Sweden.]

——, J. Langner, and L. Robertson, 1994: A mesoscale air pollution dispersion model for the Swedish west-coast region—Air pollution assessment for the year 1991. Swedish Meteorological and Hydrological Institute Reports Meteorology and Climatology 65, 27 pp. [Available from SMHI, SE-601 76 Norrköping, Sweden.]

Ramonet, M., J. C. le Roulley, P. Bousquet, and P. Monfray, 1996: Radon-222 measurements during the Tropoz II campaign and comparison with a global atmospheric transport model. *J. Atmos. Chem.,* **23,** 107–136.

Rasch, P. J., 1994: Conservative shape-preserving two-dimensional transport on a spherical reduced grid. *Mon. Wea. Rev.,* **122,** 1337–1350.

——, and D. L. Williamson, 1990: Computational aspects of moisture transport in global models of the atmosphere. *Quart. J. Roy. Meteor. Soc.,* **116B,** 1071–1090.

Robertson, L., J. Langner, and M. Engardt, 1996: MATCH—Mesoscale Atmospheric Transport and Chemistry modelling system. Basic transport model description and control experiments with ^{222}Rn. Swedish Meteorological and Hydrological Institute Reports Meteorology and Climatology 70, 37 pp. [Available from SMHI, SE-601 76 Norrköping, Sweden.]

Tremback, C. J., J. Powel, W. R. Cotton, and R. A. Pielke, 1987: The forward-in-time advection transport algorithm. Extensions to higher orders. *Mon. Wea. Rev.,* **115,** 540–555.

van Ulden, A. P., and A. A. M. Holtslag, 1985: Estimation of atmospheric boundary layer parameters for diffusion applications. *J. Climate Appl. Meteor.,* **24,** 1196–1207.

Wilkening, M. H., and W. E. Clements, 1975: Radon 222 from the ocean surface. *J. Geophys. Res.,* **80,** 3828–3830.

Wilkniss, P. E., and R. E. Larson, 1984: Atmospheric radon measurements in the Arctic: Fronts, seasonal observations, and transport of continental air to polar regions. *J. Atmos. Sci.,* **41,** 2347–2358.

Williamson, D. L., 1991: Review of numerical approaches for modeling of global transport. *Proc. 19th NATO/CCMS Int. Technical Meeting on Air Pollution Modeling and Its Application,* Creta, Greece, NATO/CCMS, 377–394.

Worthy, D. E. J., N. B. A. Trivett, J. F. Hopper, J. W. Bottenheim, and I. Levin, 1994: Analysis of long-range transport events at Alert, Northwest Territories, during the polar sunrise experiment. *J. Geophys. Res.,* **99D,** 25 329–25 344.

Zilitinkevich, S., and D. V. Mironov, 1996: A multi-limit formulation for the equilibrium depth of a stably stratified boundary layer. Max Planck Institute for Meteorology Rep. 185, 30 pp. [Available from Max Planck Institute for Meteorology, Bundesstr. 55, DE-201 46 Hamburg, Germany.]